ABSTRACT

Title of Thesis: INVESTIGATION OF THE NONLINEAR INDEX OF REFRACTION OF WATER AT 815 AND 407 NANOMETERS

Zachary W. Wilkes, Master of Science, 2007

Thesis Director: Professor Howard M. Milchberg
Institute for Physical Science and Technology

Using a highly stable spectral interferometry technique, ultrafast processes can be measured within a 2 ps temporal window. The technique was used to measure the nonlinear index of refraction due to the optical Kerr effect in water at both 815 nm and 407 nm with pump pulse lengths of ~90 femtoseconds and ~250 femtoseconds respectively. The 815 nm measurement serves as a benchmark against previous published values while the 407 nm measurement is entirely new. Knowing the value of the nonlinear index at 407 nm allows for pulse tailoring to achieve remote underwater pulse compression and self-focusing.

INVESTIGATION OF THE NONLINEAR INDEX OF REFRACTION OF WATER AT 815 AND 407 NANOMETERS

Zachary W. Wilkes

Thesis submitted to the Faculty of the Graduate School of the
University of Maryland, College Park, in partial fulfillment
of the requirements for the degree of
Master of Science
2007

Advisory Committee:
Professor Howard M. Milchberg, Chair
Professor Thomas M. Antonsen, Jr.
Professor Thomas E. Murphy

ACKNOWLEDGEMENTS

This thesis is in no way the work of one person. Time, effort, energy from many individuals went into this work.

The first people I would like to thank are Professor Howard Milchberg and Mr. Sanjay Varma. Howard served as my advisor and without his suggesting of this project, and letting me use his lab and setup none of this work would be possible. Sanjay Varma, a scholar and a gentleman, sat with me for the entire duration, late hours and weekends included, keeping the laser working, promoting quality experimentalism, and providing me with invaluable insight. I will always be in his debt.

I would also like to thank members of the Plasma Physics Division at the Naval Research Laboratory: Dr. Ted Jones and Dr. Antonio Ting. Together they provided the expertise, constructive criticism, and most importantly a "home" where I could work and grow as a scientist and engineer.

Finally I would like to thank the people that were always willing to talk to me, teach me, and keep me sane: Mr. Mike Helle, Mr. Andy York, Dr. Rich Fischer, Mr. Gregory DiComo, Mr. Yu-Hsin Chen, Mr. Alek Nacev, and Mr. Evan Merkel.

TABLE OF CONTENTS

LIST OF TABLES

LIST OF FIGURES

Chapter 1: Introduction and Overview

1.1 Introduction to Nonlinear Effects

Nonlinear optical phenomena have been observed since shortly after Maiman built his first laser, in 1960, and is considered to have begun with Franken et al. in 1961 when he observed second harmonic generation in a quartz crystal. These nonlinear optical phenomena are considered nonlinear because they occur when light, an optical field, interacts with a material and the response of that material depends nonlinearly with the strength of the optical field.

To begin an understanding of nonlinear optics, it is necessary to discuss the polarization of a material system. This polarization, or the dipole moment per unit volume, depends upon the applied optical field. In the linear, instantaneous response case, this is simply:

$$P(t) = \varepsilon_o \chi^{(1)} E(t) \tag{1.1}$$

where P(t) is the polarization, E(t) is the applied electric field, and $\chi^{(1)}$ is the linear susceptibility of the material. If the polarization is expanded as a power series to include nonlinear terms, the expression then becomes:

$$P(t) = \varepsilon_o \chi^{(1)} E(t) + \varepsilon_o \chi^{(2)} E^2(t) + \varepsilon_o \chi^{(3)} E^3(t) + \ldots \tag{1.2}$$

with $\chi^{(2)}$ the second order susceptibility and $\chi^{(3)}$ the third order susceptibility. The polarization can be further defined as:

$$P(t) \equiv P^{(1)}(t) + P^{(2)}(t) + P^{(3)}(t) + \ldots \tag{1.3}$$

where $P^{(1)}(t)$, $P^{(2)}(t)$, $P^{(3)}(t)$ are the linear polarization, second-order nonlinear polarization, and third-order nonlinear polarization respectively. It is this third order nonlinear polarization that plays the role of determining the nonlinear index of refraction.

In the case of water, one could imagine both second and third-order contributions to the total polarization thus making disentangling the second- and third-order nonlinear polarizations problematic. However, because water is a liquid with random molecular orientation and is therefore centrosymmetric (with inversion symmetry), the second-order susceptibility vanishes leaving only the third-order polarization. Thus the polarization, in the presence of an applied field, under the assumption of instantaneous electronic response for a centrosymmetric liquid, water is:

$$P(t) = \varepsilon_o \chi^{(1)} E(t) + \varepsilon_o \chi^{(3)} E^3(t) \tag{1.4}$$

$$P(t) = P^{(1)}(t) + P^{(3)}(t) \tag{1.5}$$

It is useful to get an idea of the units and possible values of the third-order susceptibility. Ordinarily $\chi^{(3)}$ is a 4th rank tensor but reduces to a scalar in a centrosymmetric, isotropic medium. A rough estimate of the size and units of $\chi^{(3)}$ is done by examining Eq. 1.4 in the regime where perturbation theory breaks down, namely where E(t) is on the order of the atomic field strength E_a and the two terms in Eq. 1.4 are comparable in magnitude giving us:

$$\chi^{(1)} E_a \approx \chi^{(3)} E_a^3 \text{ or } \chi^{(3)} \approx \frac{\chi^{(1)}}{E_a^2} \tag{1.6}$$

For condensed matter[7] $\chi^{(1)}$ is on the order of 4π, dimensionless, (in esu. units on the order of 1, dimensionless) and therefore $\chi^{(3)}$ is inversely proportional to E^2_a.

Assuming a Bohr-like atom then the magnitude of the atomic field strength is:

$$|E| = \frac{1}{4\pi\varepsilon_o} \frac{q}{a_o^2} \tag{1.7}$$

where q is the unit charge of an electron, ε_o is the permittivity of free space, and a_o is the Bohr radius. This yields $E_a = 5.13\text{x}10^{11}$ V/m with $\chi^{(3)} \approx 4.8\text{x}10^{-23}$ $m^{2/}$ V^2.

1.2 Linear and Nonlinear Index of Refraction

Using a classical anharmonic oscillator system along with perturbation theory, expressions for the linear susceptibility and third-order nonlinear susceptibility can be derived. This provides a classical approach to the index of refraction due to the linear and third-order nonlinear susceptibilities.

Beginning with a mass on a spring classical harmonic oscillator (Figure 1.1), the equation of motion can be written as:

$$\ddot{x}(t) + 2\gamma\dot{x}(t) + \Omega^2 x(t) = -\frac{e}{m}E(t) \tag{1.8}$$

where E(t) is the applied electric field, $m\Omega^2 x$ is the restoring force and $2m\gamma\dot{x}$ the damping force. Ω is the resonant frequency such that $\Omega^2 = k/m$.

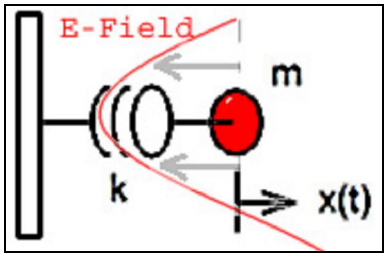

Figure 1.1: A classical harmonic oscillator with an E-field perturbing an electron "on a spring".

From this model, a linear electric susceptibility and linear index of refraction can be found (see Appendix D) to be:

$$\chi^{(1)}(-\omega;\omega) = \frac{Ne^2}{m\varepsilon_o}\frac{1}{D(\omega)} \tag{1.9}$$

$$n_o = \left(1 + \frac{Ne^2}{m\varepsilon_o D(\omega)}\right)^{\frac{1}{2}} \tag{1.10}$$

N is the density of atoms per unit volume, e is the charge of an electron, m = mass of an electron, $D(\omega) = \Omega^2 - 2i\gamma\omega - \omega^2$, and ε_o is the permeability of free space.

In order to derive the nonlinear index of refraction, perturbation theory can be used along with the classical anharmonic oscillator model.

Consider first an anharmonic oscillator with, in addition to a linear restoring force kx(t), there is a lowest order nonlinear contribution $k_3x^3(t)$. Force contributions in even powers of the displacement x(t) are dropped because they derive from potential terms that are odd functions of x(t) and these are forbidden owing to our assumption of a centrosymmetric medium.

$$m\ddot{x}(t) = -eE(t) - \left(k_1 x(t) + k_3 x^3(t)\right) - 2m\gamma\dot{x}(t) \tag{1.11}$$

Using perturbation theory, it is possible to show (see Appendix D) that the third order susceptibility is given by:

$$\chi^{(3)}(-\omega;\omega,\omega,-\omega) = \frac{-Ne^4 k_3}{m^4\varepsilon_o D^3(\omega)D^*(\omega)} \tag{1.12}$$

where N is the density of atoms per unit volume, e is the charge of an electron, m = mass of an electron, $D(\omega) = \Omega^2 - 2i\gamma\omega - \omega^2$, $D^*(\omega)$ = complex conjugate of $D(\omega)$, and ε_o is the permeability of free space. This model assumes the atoms are non-interfering which is reasonable for water because the intramolecular forces on the bound electrons greatly exceed the intermolecular forces.

Equation 1.12 gives an expression for the nonlinear susceptibility; however, it is incomplete as a value because k_3 is not a known quantity. Using equations 1.9 and 1.12

an expression for the total index of refraction, n, in terms of susceptibilities can be found (Appendix D). If we define a nonlinear index of refraction n_2 by:

$$n = n_o + n_2 I \tag{1.13}$$

where I is the intensity = $(n_o \varepsilon_o c|E(\omega)|^2)/2$, then n_2 is given in terms of the underlying susceptibility by:

$$n_2 = \frac{3\chi^{(3)}(-\omega;\omega,\omega,-\omega)}{4n_o^2 \varepsilon_o c} \tag{1.14}$$

1.3 Cross Phase Modulation

Our interferometric technique employs cross phase modulation in which two beams, one of weak intensity (probe) and one of strong intensity (pump), propagate in a medium such that the strong beam influences the accumulated propagation phase of the weak beam (Figure 1.2).

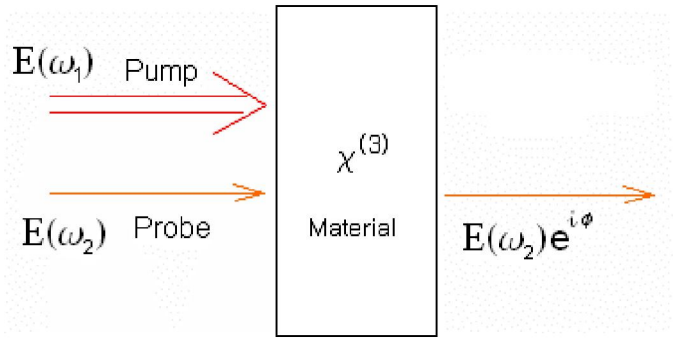

Figure 1.2: A strong pump $E(\omega_1)$ and weak probe $E(\omega_2)$ interacting in a nonlinear $\chi^{(3)}$ material inducing a phase shift ϕ on the weak probe by cross-phase modulation (XPM).

When considering the cross-phase modulation (XPM) effect there is a degeneracy factor[8] of 3/2 when the pump and probe beam are linearly polarized and parallel. This is different from the 3/4 (Equation 1.13) degeneracy factor for the self-phase modulation effect. The nonlinear polarization, $P^{(3)}_{xpm}(\omega_2)$, (Equation 1.15) and nonlinear index of

refraction (Equation 1.16) seen by the weak probe beam is:

$$P_{xpm}^{(3)}(\omega_2) = \frac{3\varepsilon_o}{2}\chi^{(3)}(-\omega_2;\omega_2,\omega_1,-\omega_1)E(\omega_2)E(\omega_1)E^*(\omega_1) \tag{1.15}$$

$$n_{\omega 2} = n_o(\omega_2) + n_2^{xpm} I(\omega_1) \tag{1.16}$$

where $n_{\omega 2}$ denotes the index of refraction seen by the probe beam, $n_o(\omega_2)$ is the linear index of refraction of the probe beam, $E(\omega_1)$ is the electric field phasor at the pump frequency, $E(\omega_2)$ is the electric field phasor at the probe frequency, ε_o the permittivity of free space, $\chi^{(3)}$ is the nonlinear susceptibility, $I(\omega_1)$ is the intensity of the field at the pump frequency, and n_2^{xpm} is the cross-phase modulation nonlinear index of refraction. When the pump and probe beams are linearly cross-polarized, the degeneracy factor becomes 2/3 (see Appendix C for a brief derivation). Below is a list of how degeneracy factors affect the index of refraction for self-phase and cross-phase modulation effects:

$$n_{\omega 1} = n_o(\omega_1) + n_2^{spm} I(\omega_1) \tag{1.17}$$

$$n_{\omega 2-parallel} = n_o(\omega_2) + 2n_2^{spm} I(\omega_1) \tag{1.18}$$

$$n_{\omega 2-perpendicular} = n_o(\omega_2) + \frac{2}{3} n_2^{spm} I(\omega_1) \tag{1.19}$$

where $n_{\omega 1}$ = total index of refraction experienced by a strong pump during self-phase modulation, $n_{\omega 2\text{-parallel}}$ is the total index of refraction experienced by a weak probe during cross-phase modulation of two linearly polarized parallel beams, $n_{\omega 2\text{-perpendicular}}$ is the total index of refraction experienced by a weak probe during cross-phase modulation of two linearly polarized perpendicular beams, $n_o(\omega_x)$ is the linear index of refraction at ω_x where x =1 for the strong pump and x = 2 for the weak probe, and n_2^{spm} is the nonlinear index of refraction due to self-phase modulation as seen in Equation 1.14. It should be

noted that the factor between parallel and perpendicular polarization for cross-phase modulation is 3 and therefore one would expect a 3x reduction in phase shift for a perpendicularly polarized probe.

By using cross-phase modulation phenomena, it is possible to get a value for the nonlinear index of refraction by observing and measuring the phase shift in the probe beam. Consider the following equations: for the background phase ϕ_{bg} (no cross phase modulation) and phase ϕ_{xpm} with cross-phase modulation

$$\phi_{bg} = k_{bg} z - \omega t \tag{1.20}$$

$$\phi_{xpm} = k_{xpm} z - \omega t \tag{1.21}$$

The difference between the two phase shifts, when measured, can be used to obtain a value for the nonlinear index of refraction of the medium. For a pulse finite in the transverse direction, finite in time, and changing over the interaction length the phase shift between the background and XPM beams is:

$$\Delta\phi(x,t) = \frac{\omega}{c} n_2 \int_0^z I(x, z', t) dz' \tag{1.22}$$

Using a method outlined below, this phase shift is measured and the effective nonlinear indices of refraction are obtained for red (815 nm, 90 fs FWHM) and blue (407 nm, ~250 fs FWHM) light pulses.

1.4 Spectral Interferometry Measurement Technique

Previous work in measuring the nonlinear index of refraction has been done by elliptical polarization rotation (EPR)[16], spatial profile analysis (SPA)[17] and spectral analysis of self-phase modulation[18][21]. Another method involves determining the critical power, P_{crit}, for self-focusing and then back calculating to get the effective n_2

value[3][19]. Here, the technique used to measure the instantaneous and effective nonlinear index of refraction in water was supercontinuum spectral interferometry (SSSI).

Spectral Interferometry (SI) is useful as a measurement technique because it is a phase sensitive linear diagnostic[25] capable of measuring transient nonlinear indices of refraction. Key to this technique is the use of collinear reference-probe pulse interference. The weak reference pulse precedes the pump, followed by replica probe pulse and the pump all collinearly aligned. The probe pulse temporarily overlaps the pump. The strong pump and weak probe interact in a medium resulting in a phase shifted probe which is then interfered in the frequency domain with its previously identical reference probe in a spectrometer. From this interference small phase shifts can be detected. In the earliest version of SI, pump-induced transients to the medium's refractive index were measured by shot-to-shot temporal scanning of the probe with respect to the pump. In order for this method to give high quality temporal results, a high degree of shot-to-shot stability of both the pump and probe pulses was needed to reconstruct the index transient. This often proved difficult to achieve.

When single-shot SI (SSI) was first developed, it incorporated a linear chirp to the reference and probe allowing the index transient phase shift to be detected by each slice of the chirp[25]. These could then be interfered in a spectrometer where direct mapping between frequency and time allowed the temporal phase variation to be extracted. However, this method was limited by both bandwidth (the probe pulse was obtained from the same Ti:Sapphire laser providing the pump pulse) and by direct mapping distortions to the recovered transient, especially for large chirps.

Both of the above problems were solved by reference [13] which introduced broad

spectrum supercontinuum (SC) probe and reference pulses generated by self-focusing in a Xenon gas cell. By producing a spectrum of 100 nm or greater, a temporal resolution of 10 fs can be obtained[25]. Using this single-shot supercontinuum spectral interferometry (SSSI) requires knowledge of $\tilde{E}_{pr}(\omega) \propto \sqrt{I_{pr}(\omega)}, \tilde{E}_{r}(\omega) \propto \sqrt{I_{r}(\omega)}$ and $\phi_r(\omega)$, where $I_{pr}(\omega)$ and $I_r(\omega)$ are the probe and reference intensities measured by spectrometer and $\phi_r(\omega)$ is the reference phase measured by cross-phase modulation[12] (XPM). Performing a Fourier transform on the reference-probe interferograms allows extraction of the time domain phase shift, $\Delta\phi(x,t)$, imparted on the probe beam, $E_{pr}(x,t)\exp(i\Delta\phi(x,t))$, where x is the spatial coordinate transverse to the interaction and along the spectrometer entrance slit. From $\Delta\phi(x,t)$, the change in refractive index, and thus $n_2(x,t)$, caused by XPM from a pump beam can be obtained from Equation 1.22 as discussed above.

1.5 Conclusion

Our SSSI technique, having solved the problems of single-shot spectral interferometry, will provide good time resolution (~10 fs) to make a measurement of the nonlinear index of refraction of water for 815 nm and 407 nm as well as a 2 ps time window to observe possible delayed nonlinear responses. The calculated value for 815 nm will be benchmarked against published data while the 407 nm value will be used in modeling and experimentation at the Naval Research Laboratory for remote underwater pulse compression.

Chapter 2: Water Cell and Water Cell Housing

2.1 Design and Construction of Water Cell and Housing

The thin cell water apparatus consists of two distinct components. The first component is, the water cell (WC). This is consists of two, 240 μm pieces of fused silica (the windows) and four plastic spacers either 1.8 mm or 3.2 mm thick. The plastic was chosen because it is rigid, easy to cut, and easy to shape. The shape of the cell is a square measuring 1.4 cm x 1.4 cm. Two opposite sides of the square are closed and two opposite sides have 6 holes, 2 mm in diameter (1.6 mm for the smaller cell) allowing water to flow (Figure 2.1).

The second component is, the water cell housing (WCH). The WCH, Figure 2.2, is composed of a Kwik-Flange blank and a Kwik-Flange unbored stub. Both of these were modified to accommodate the 3.2 mm water cell and the 1.8 mm water cell. These two pieces fit together like a clam shell and are clamped together with an aluminum quick-flange clamp. The WCH, composed of stainless steel, will not contact the water cell but will instead have size 207 O-rings which seal against the stainless steel and the window. Grooves are cut to 0.087" and 0.115" deep for the 1.8 mm and 3.2 mm water cells respectively for the O-rings. In the Kwik-Flange stub three holes are drilled, see Figure 2.3, one hole in the center for the laser pulse to propagate to the WC and two diametrically opposite holes to allow water flow. In the Kwik-Flange blank only one hole is drilled in the center to allow the laser to exit the WCH. Figure 2.4 is a photograph of the WCH during the experiment and shows a slightly off-axis view of the laser beam-axis through the WCH. See Appendix G for schematics and 3-D CAD drawings.

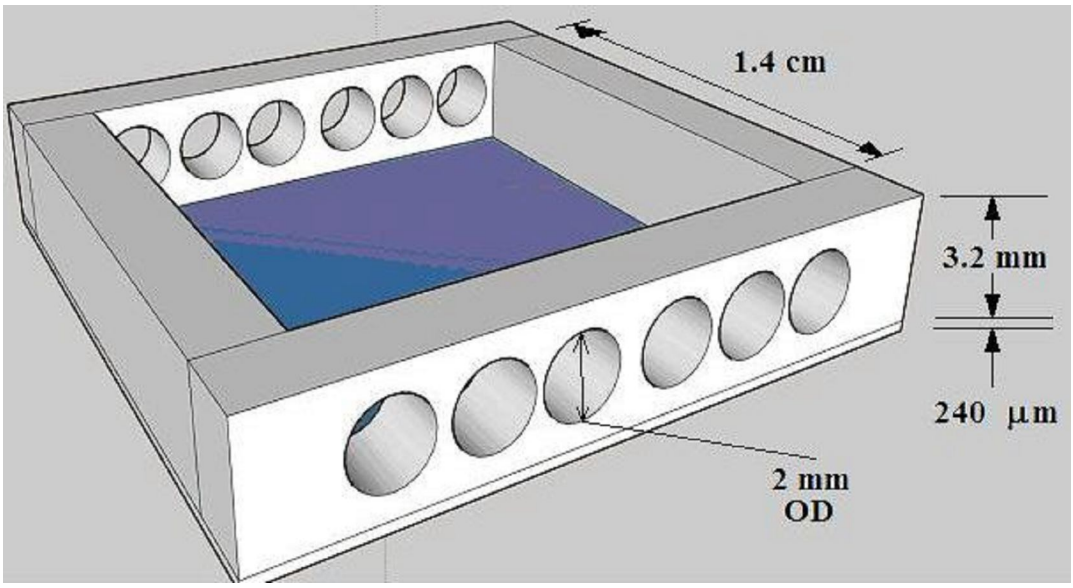

Figure 2.1: A to-scale 3-D rendering of the WC composed of 4 plastic spacers, 2 of which have through holes cut for water flow. The bottom plate is a 240 µm fused silica window. Not shown is the top fused silica window. The WC is placed inside the WCH.

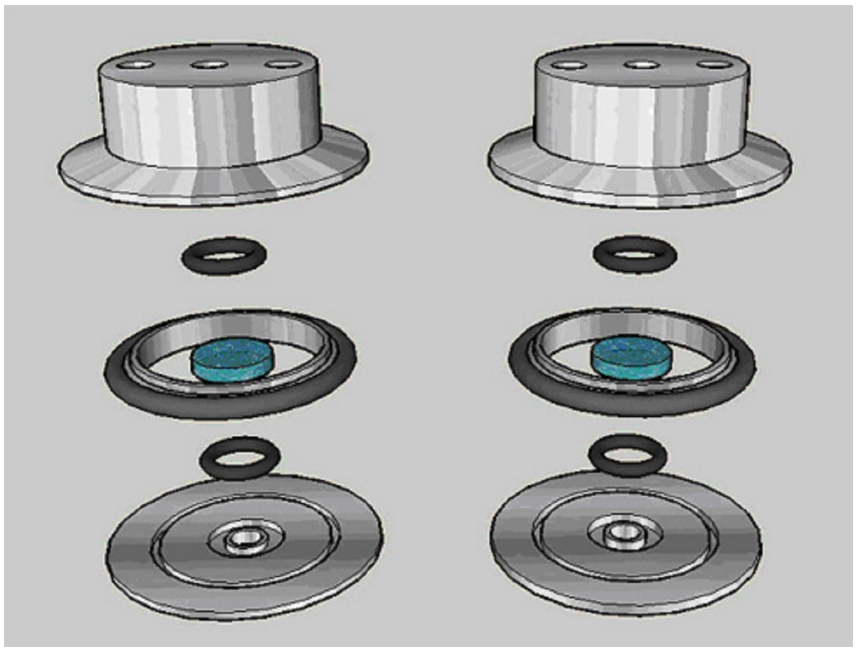

Figure 2.2: 3-D breakaway rendering of the WCH and WC (blue disks) separated into components. The black size 207 O-rings fit in the grooves and seal against the windows of the water cell (blue) while a KF centering assembly (large black ring) uses a large O-ring to seal the water cell chamber. The 1.8 mm WC is on the left, 3.2 mm on the right.

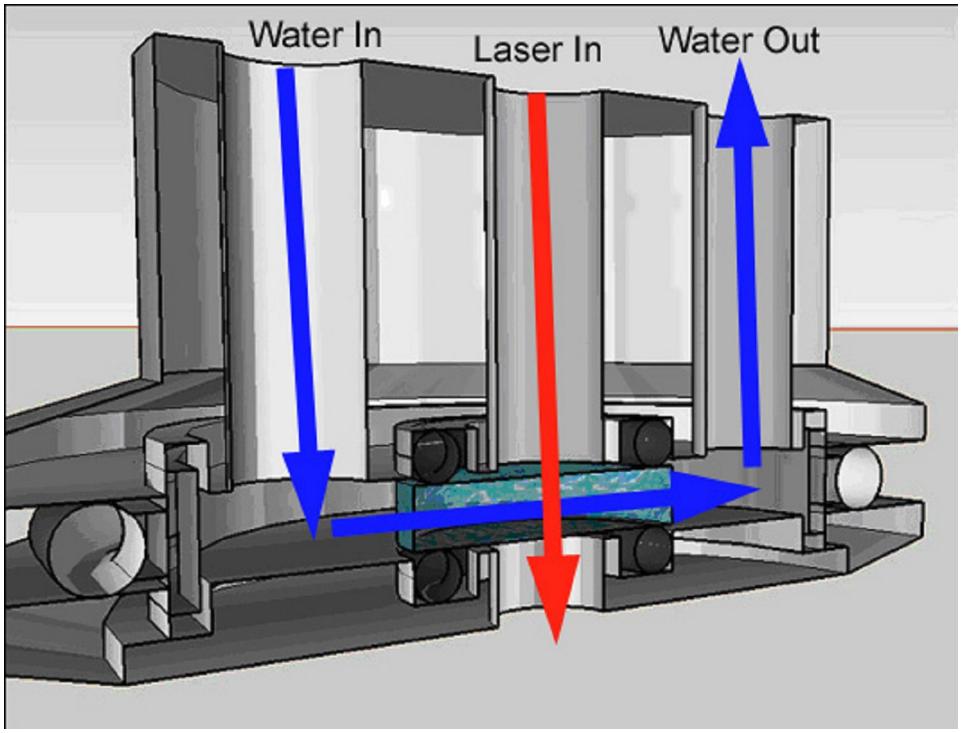

Figure 2.3: A 3-D cutaway of the WCH and WC with arrows depicting the water flow (blue arrows) and laser path (red arrow). The black O-rings seal against the WCH and WC windows.

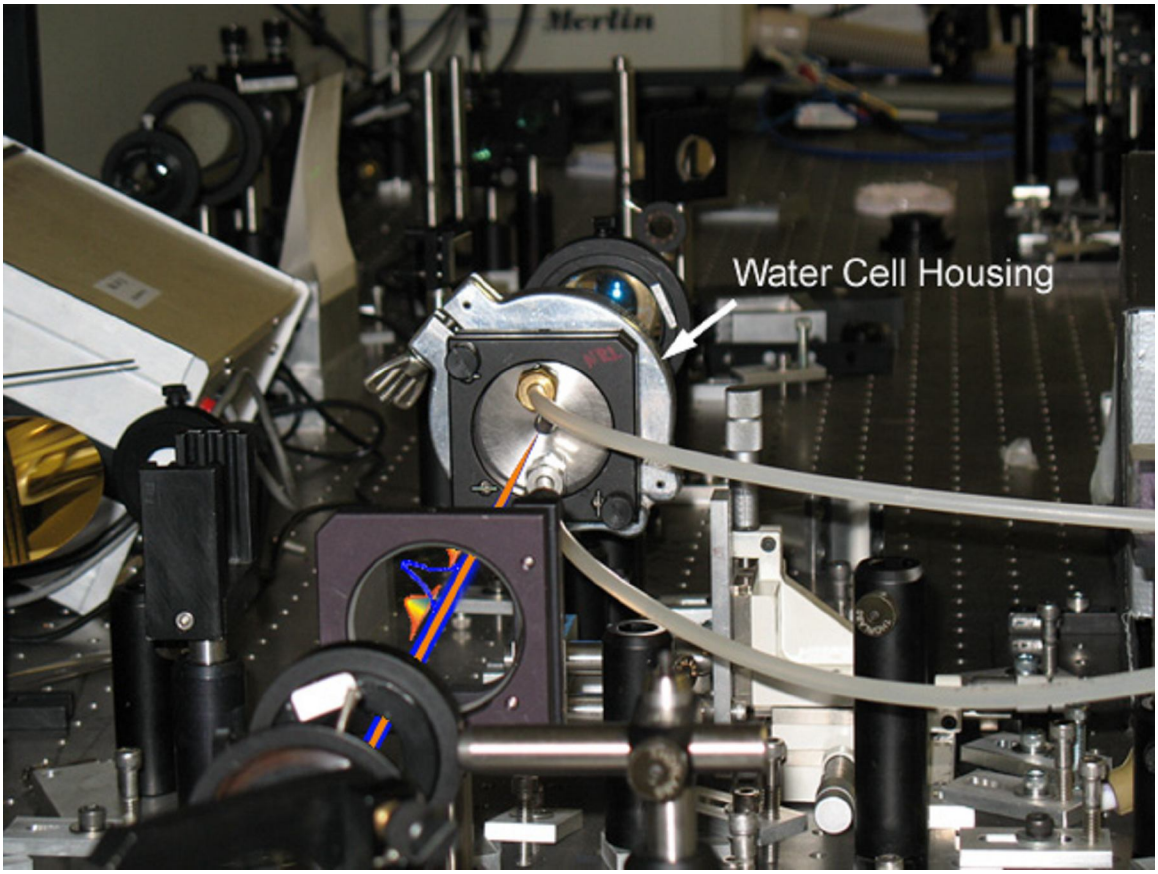

Figure 2.4: A photograph showing the SC (orange) and pump (blue) pulse paths to the water cell in the lab setup.

2.2 Structural Integrity of the Water Cell

Modeling the water cell in the program COMSOL provides CAD-like images showing the stresses and strains of the water cell under a given pressure, in the test case 5 psi. The consideration is the stress and strain applied to the fused silica surface by the rubber O-rings which are used to seal the fused silica surface against the stainless steel when the cell is placed inside the WCH. Of interests is the maximum stress the fused silica will undergo given the O-ring to fused silica surface geometry. According to published values[5], the ultimate strength of fused silica is about 50 MPa. However, it is common to consider a safety factor of 2 when determining the effect of an applied pressure such that a stress point of 25 MPa would be considered dangerous. The

following figures are from the COMSOL print out and show the geometry used and the final result of stress points.

Another important factor directly relating to the accuracy of the phase shift data is the flex of the window under pressure. When the water cell was simulated with the COMSOL program, the flex of the fused silica pane was roughly 5 μm before the pane reached a breaking pressure. A flex of 5 microns for both windows over a cell of either 3.2 mm or 1.8 mm gives a change in path length of roughly 0.3% for the 3.2 mm cell and 0.56% for the 1.8 mm water cell. Since the flex of 5 μm happens at the safety factored breaking point, which will not be the operating point, and since the effect is insignificant, the flex of the windows will not need to be considered in nonlinear index of refraction calculation.

From the stress image (Fig. 2.7) the maximum stress at a single point was 23.12 MPa. This is very close to the safety factored ultimate strength of 25 MPa. Therefore a pressure of 5 psi would most likely break the fused silica along an O-ring to fused silica interface. In order to help guard against this, a 2 psi safety valve could be placed on the water flow line to guard against over pressurizing the water cell and breaking the window.

In conclusion the effect of the flex from the water cell can be ignored and the water cell will approach a breaking pressure should 5 psi be applied to the cell. Over pressurizing the water cell can be combated by providing a bleed-off valve rated at 2 psi.

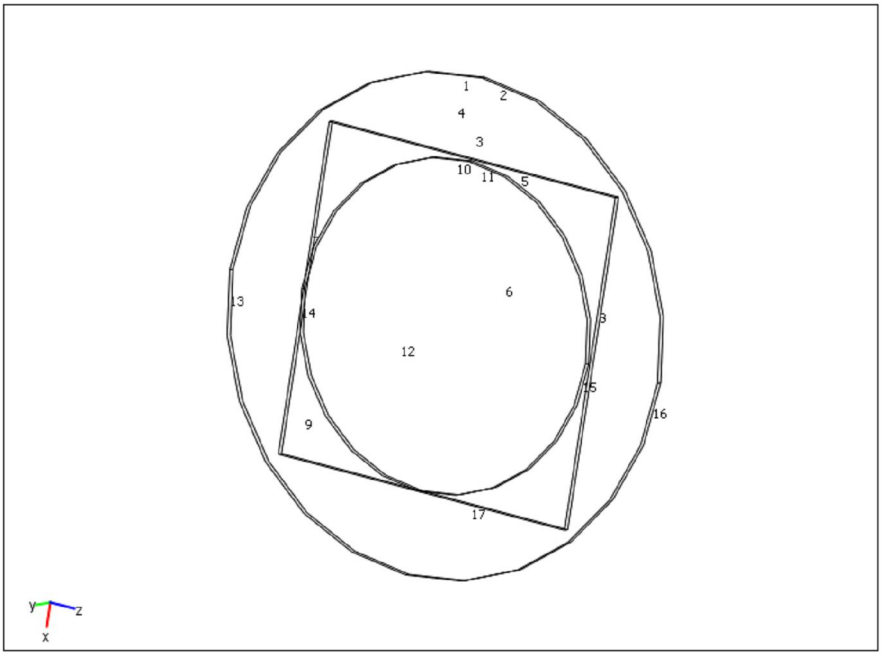

Figure 2.5: COMSOL framing image of water cell window (square) against the O-ring (concentric circles) used to produce a system of stresses and strains in the simulation.

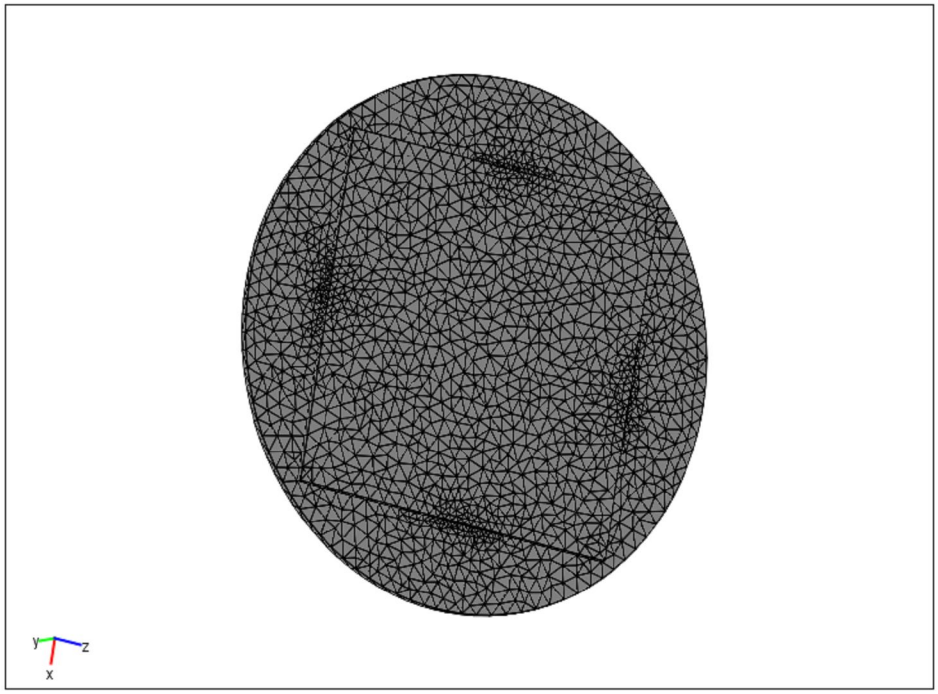

Figure 2.6: COMSOL mesh image dividing the system into small geometries in order to calculate stresses and strains of the window on the O-ring given 5 psi of pressure.

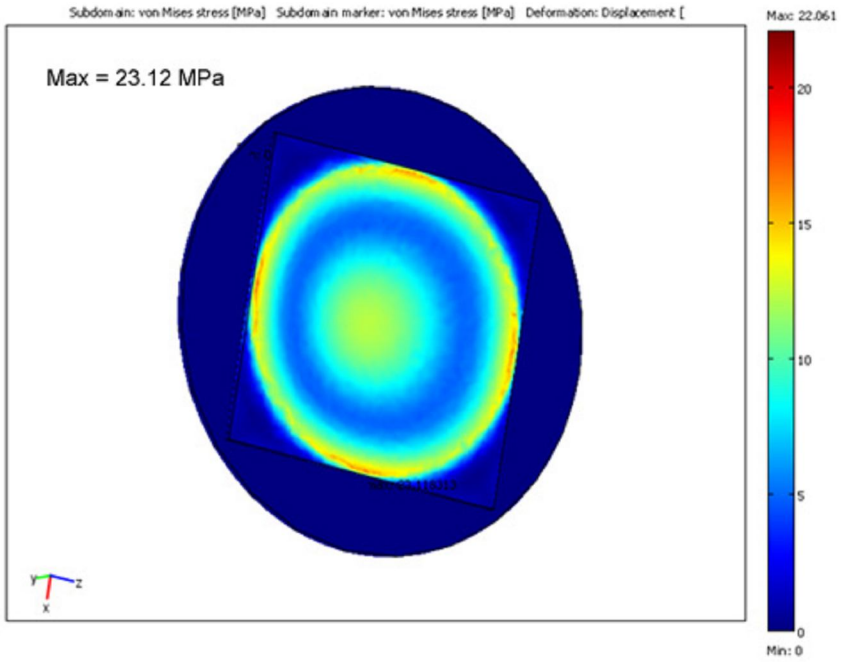

Figure 2.7: False color image showing regions of maximum stress in megaPascals of the window on the O-ring under 5 psi of pressure. The peak pressure, 23.12 MPa, occurs at a joint between the O-ring and edge of the window. The is very close to the safety factored 25 MPa. The flex in the window is about 5 μm.

2.3 Temperature Induced Phase Shift

Aside from the cross phase modulation effect, other effects in the water itself could change the index of refraction and produce a phase shift unrelated to the cross phase modulation effect. Of greatest concern is the index of refraction change due to a temperature change from shot-to-shot, or over several shots, so that the phase shift becomes a function of temperature. The laser to be used is a 1kHz - 815 nm Ti:Sapphire laser and therefore within 1 second one-thousand laser shots will impinge upon the sample and could have an appreciable effect on the index of refraction.

The 815 nm case is the most pertinent because at 815 nm the absorption[1] of distilled water, ~ 2.0×10^{-2} cm^{-1}, is much greater than the pure water absorption[28] at 407 nm ~5.0×10^{-5} cm^{-1}

Given a laser pulse of energy = 5 μJ, $1/e^2$ diameter 120 μm, and 90 fs full-width-at-half-maximum pulse length, the following calculations can be made:

$$Power = \frac{5\mu J}{90\, fs} = 5.56x10^7\, W \tag{2.1}$$

$$I_{out} = I_{in} e^{-\alpha z} \tag{2.2}$$

where I_{out} is the output intensity, I_{in} is the input intensity, z is the interaction length, α is absorption coefficient in Beer's Law. This can be written in terms of power as:

$$P_{out} = P_{in} e^{-\alpha z} \tag{2.3}$$

This is valid if the spot size remains virtually unchanged, a valid assumption for the experimental geometry used. The peak power of a single pulse is P_{in} = 55.6 MW.

$$P_{absorbed} = P_{in} - P_{out} \tag{2.4}$$

$$P_{absorbed} = P_{in}\left(1 - e^{-\alpha z}\right) \tag{2.5}$$

For a water path of 3.2 mm the energy absorbed, per pulse, is approximately $3.3x10^{-8}$ Joules. Assuming all the absorbed energy goes into heat, which remains in the interaction volume without dissipation before the next pulse (at the laser pulse repetition rate of 1 kHz), then it is necessary to provide fresh water for each shot. This is shown below.

The heat change formula gives the change in temperature of a mass of water for a given amount of energy:

$$\Delta Q = mC\Delta T \tag{2.6}$$

From this a change in index of refraction due to energy deposited in the water cell from a single pulse is calculated (see Appendix E) to be $\Delta n = 2x10^{-8}$. Taking into account the 1 kHz operation yields a $\Delta n = 2x10^{-5}$ after 1 second of interaction. This is

comparable to the shot-to-shot nonlinear index change of $\delta n = 5x10^{-5}$:

$$n = n_o + \delta n \tag{2.7}$$

$$\delta n = n_2 I \tag{2.8}$$

If the intensity of the pulse is $I \approx 5x10^{11}$ W/cm^2, and the n_2 value[3] at 815 nm is on the order of 10^{-16} this gives an intensity induced change of index of refraction:

$$\delta n = n_2 I = 10^{-16} * 5x10^{11} = 5x10^{-5} \tag{2.9}$$

Since the laser is operating at 1 kHz, this means that within 1 second the change in index of refraction from deposited energy will be $\Delta n = 2x10^{-5}$ which is appreciable to the change in index from nonlinear effects. This result means that the water must flow in order to allow the laser pulse to interact with "fresh" water. A safe flow velocity to introduce fresh water to each pump pulse is 0.2 m/s as shown below.

2.4 Water Cell Design – Reynolds Number

Another factor for the possibility of changing the index of refraction or influencing the phase shift seen by a passing pulse is the density of the water. Since the water will be flowing through the water cell, there is a chance it could become turbulent at the required velocity for keeping temperature effects negligible. If the water is turbulent, there is a chance for density fluctuation during pulse interaction. To determine whether the water flowing through the cell is turbulent the following calculation is used.

The water cell consists of either a 1.8mm or 3.2 mm thick spacer between two pieces of 240 μm thick fused silica. The proposed velocity of the water is as follows: for a spot size of ~100 μm, a safe velocity to provide fresh water would move this spot 2 full pump spots away (Figure 2.8) within a time of 1 millisecond.

$$v = \frac{200\mu m}{1ms} = 0.2\,m/s \tag{2.10}$$

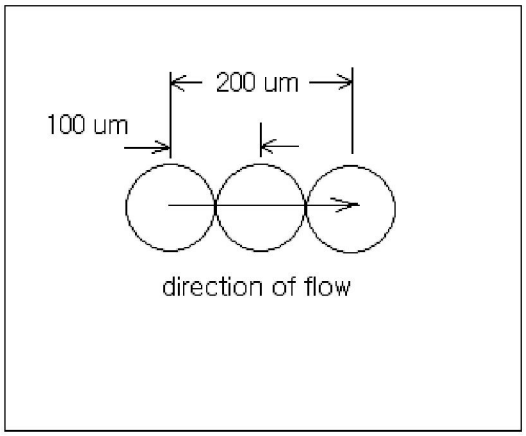

Figure 2.8: Diagram of heated volume of water moving through the water cell. A safe velocity based on the laser operating frequency and size of spot is v = 0.2 m/s.

This is the velocity through the optical interaction region (between the fused silica plates) but not through the holes at the ends. In order to maintain a velocity of 0.2 m/s through the optical interaction region, the velocity through the holes can be determined by the following:

$$A_{IX} = (3.2mm)(1.4cm) = 44.8\ mm^2 \tag{2.11}$$

$$A_{HX} = 6(\pi(1mm)^2) = 6\pi\ mm^2 \tag{2.12}$$

A_{IX} is the cross-sectional area of the interaction region and A_{HX} is the cross-sectional area of interaction for the six holes. In order to maintain the desired velocity, then the following is true:

$$v_I A_{IX} = v_H A_{HX} \tag{2.13}$$

where v_I = velocity through the interaction region and v_H is the velocity through the holes. Solving this gives the velocity through the holes to be.

$$(0.2m/s)(44.8mm^2) = (6\pi mm^2)(v_H) \tag{2.14}$$

$$v_H = 0.475\ m/s \tag{2.15}$$

The velocities through the interaction region and through the holes are important in determining the Reynolds number to ensure laminar flow.

The formulae needed to determine the Reynolds Number[4] for the water cell orifices are the following:

$$R_{holes} = \frac{\rho v_s D}{\mu} \tag{2.16}$$

$$R_{cell} = \frac{\rho v_s D^*}{\mu} \tag{2.17}$$

where ρ = density of liquid, v_s = the mean fluid velocity, μ = the fluid viscosity, and D, D^* are the characteristic lengths. For the holes, the characteristic length is the hole diameter because they are tubes with circular cross-sections. For the cell which has a rectangular cross-section, the characteristic length is:

$$D^* = \frac{4A_x}{u} \tag{2.18}$$

where A_x = cross-sectional area and u = the perimeter of the cross-sectional area. The characteristic length of the cell is D^* = 5.208 mm. Using this the Reynolds numbers for the holes and the cells are:

$$R_{holes} = 950 \tag{2.19}$$

$$R_{cell} = 1040 \tag{2.20}$$

For water flow through a tube, a Reynolds number between 2000 and 3000[4] would indicate turbulent flow. The Reynolds numbers obtained for the 3.2 mm water cell and associated flow tubes are well below the turbulent flow. It should be noted that the proposed velocity of 0.2 m/s is actually twice as fast as necessary. When calculating the Reynolds numbers for the 1.8mm cell, the following values are obtained:

$$R_{holes} = 1070 \quad (2.21)$$

$$R_{cell} = 640 \quad (2.22)$$

Again, these numbers are safe for being non turbulent.

2.5 Conclusion

The water cell, composed of 1.8 and 3.2 mm spacers with 240 μm fused silica windows removes unwanted temperature effects by allowing water to flow and also provides a short interaction length to avoid self-focusing. This cell is housed in a robust stainless steel housing, custom machined, to allow for the different water cell thicknesses and the water flow. By using Reynolds number calculations the flow through the water cell will be not be turbulent.

Chapter 3: Simulation of Pulse Interaction

3.1 Simulation of the beam in Fused silica windows and Water

Before performing the experiment, a simulation of the beam passing through the windows and water was done using MATLAB (see Appendix A). The simulation involves using the following pulse evolution equations laid out by Sprangle et al.[6]

$$\frac{\partial^2 R}{\partial z^2} = \frac{4}{k_o^2 R^3}\left(1 - \frac{E_o}{\tilde{P}_{NL}}\frac{1}{T}\right) \tag{3.1}$$

$$\frac{\partial^2 T}{\partial z^2} = \frac{4\beta_2}{k_o}\frac{E_o}{\tilde{P}_{NL}}\frac{1}{R^2 T^2} + \frac{4\beta_2^2}{T^3} + \frac{1}{\beta_2}\frac{\partial \beta_2}{\partial z}\frac{\partial T}{\partial z} \tag{3.2}$$

where R is the spot size, k_o is the vacuum wave number, T(z) is the laser pulse duration as a function of propagation distance, β_2 is the group velocity dispersion parameter, $\tilde{P}_{NL}$ is the effective nonlinear self-focusing power equal to:

$$\tilde{P}_{NL} = \frac{\lambda_o^2}{8\pi n_o n_2} \tag{3.3}$$

where the usual self-focusing power $P_{NL} = 4^* \tilde{P}_{NL}$. $E_o = PT$ is independent of z and is proportional to the pulse energy where P = initial peak power in Watts.

The code was originally developed for pulse propagation through air but can be extended to water and fused silica. The equations arise from the assumption that the pulse is self-similar[6] –that it always remains a Gaussian in space and time with well characterized spot size and pulse duration. The complex field is given by:

$$A(r,z,\tau) = B(z)e^{i\theta(z)}e^{-[1+i\alpha(z)]r^2/R^2(z)}e^{-[1+i\beta(z)]\tau^2/T^2(z)} \tag{3.4}$$

where B is the field amplitude, β is the chirp parameter, α is a variable related to the curvature of the wave front, θ is the phase, and R is the spot size, and T is the pulse

length. Substitution into the nonlinear wave equation and matching real and imaginary parts results in Equations 3.1 and 3.2. Equations 3.1 and 3.2 are coupled, second-order differential equations, solving them in MATLAB requires making the equations first-order differential equations. In Equation 3.2 $\frac{\partial \beta}{\partial z} = 0$ since the material is assumed to be uniform in z.

In order to closely model the pulse propagation, physical parameters are required for the group velocity dispersion of both fused silica and water at 815 nanometers and 407 nm as well as nonlinear indexes of refraction, and pulse parameters. The following table summarizes the various parameters used in the simulation.

Water	Red	Blue	units
λ	815	407	nm
n2	2.0E-016	4.0E-016	cm^2/W
GVD	2.48E-028	1.00E-027	s^2/cm
n_o	1.33	1.339	-
energy	60	10	uJ
spot size	150	150	um - FWHM
Glass (FS)	Red	Blue	units
λ	815	407	nm
n2	2.48E-016	3.25E-016	cm^2/W
GVD	3.50E-028	9.60E-028	s^2/cm
n_o	1.45	1.4696	-

Table 3.1

The value for the nonlinear index of refraction for 815 nanometer light is from Liu et al.[3]. Values for the nonlinear index of refraction for fused silica at 800 and 400 nanometers are from [21]. GVD values for fused silica are calculated from the Sellmeier equation. The GVD value for 407 nm in water was experimentally determined at NRL by Dr. Ted Jones. The GVD value for 815 nm light was found at [29]. The nonlinear index of refraction value for 407 nm in water is from critical focusing power calculations.

As the beam propagates, the spot size and pulse duration change. In order to keep the simulation accurate, the energy remains constant as the pulse propagates. Since the paper uses E_o which is proportional to the actual energy, the actual energy needs to be scaled to the E_o and this number is to be kept constant.

The purpose of the simulation is to model optical compression dynamics and predict whether the pulse reaches ionization intensities. The simulation does not include Raman effects or linear absorption. Figures 3.1-4 show the results of the simulation.

The initial pulse parameters were R_o = 150 μm at full-width-at-half-maximum (FWHM) spot and 90-femtosecond (FWHM) pulse length. Converting to $1/e^2$ values gives the initial spot R(z=0) = 127.4 μm and initial pulse length T(z=0) 153 fs. Conversion to the $1/e^2$ numbers was done because those are the values considered in the above Equations 3.1 and 3.2.

Figure 3.1 shows the pulse radius change, R(z) due to nonlinear self-focusing through the entrance and exit 240 μm fused silica windows and 3.2 mm water cell. The pulse compresses due to nonlinear effects from 150 μm FWHM to 142 μm FWHM.

Figure 3.2 shows the pulse length T(z) change as predicted by Equation 3.2 through the entrance and exit 240 μm fused silica windows and 3.2 mm water cell. The pulse lengthens from 90 fs FWHM to 107 fs. In both simulations the fused silica windows provide very little contribution to the pulse shaping.

A plot of the intensity through the water, Figure 3.3, shows the pulse intensity is below the ionization threshold intensity of a 100 femtosecond 580 nanometer pulse as given by Noack and Vogel[9] of 1.11×10^{13} W/cm^2. Although the wavelength is different it serves as a good measure of ionization threshold, I_{th}, because the 100 fs pulse length

puts the process near the wave-length independent tunneling ionization regime.

According to Liu[3] the water breakdown threshold for a 45 femtosecond 810 nm pulse is ~8.8×10^{12} W/cm^2. Therefore it will be safe to stay at least one order of magnitude below I_{th} to avoid breakdown, plasma generation, and unwanted effects.

The simulation shows a decreasing pulse intensity through the water. This is because, given the particular pulse parameters of the simulation, the group velocity dispersion effect of temporally stretching the pulse reduces the intensity faster than nonlinear focusing can increase it. GVD appears to be the dominant factor in pulse broadening because of the nearly linear pulse broadening, seen in Figure 3.3. Figure 3.4 shows the pulse length T(z) and pulse radius R(z) normalized to their initial values entering the water.

3.2 Conclusion

The simulation was done with different parameters (primarily energy and spot size) than the actual experiment. The parameters in the simulation were chosen based on energies much higher (~100x) than the experimental energies in order to showcase the self-focusing and dispersion effects which occur in pulse propagation through water. Results from the simulation are not indicative of the experimental results beyond showing that ionization intensities can be avoided. Also, the author of this paper used the simulation as an educational exercise to learn about self-focusing and dispersion effects. Modeling of the experimental parameters would give no new or interesting behavior because experimental peak powers were equal to or less than the critical self-focusing power.

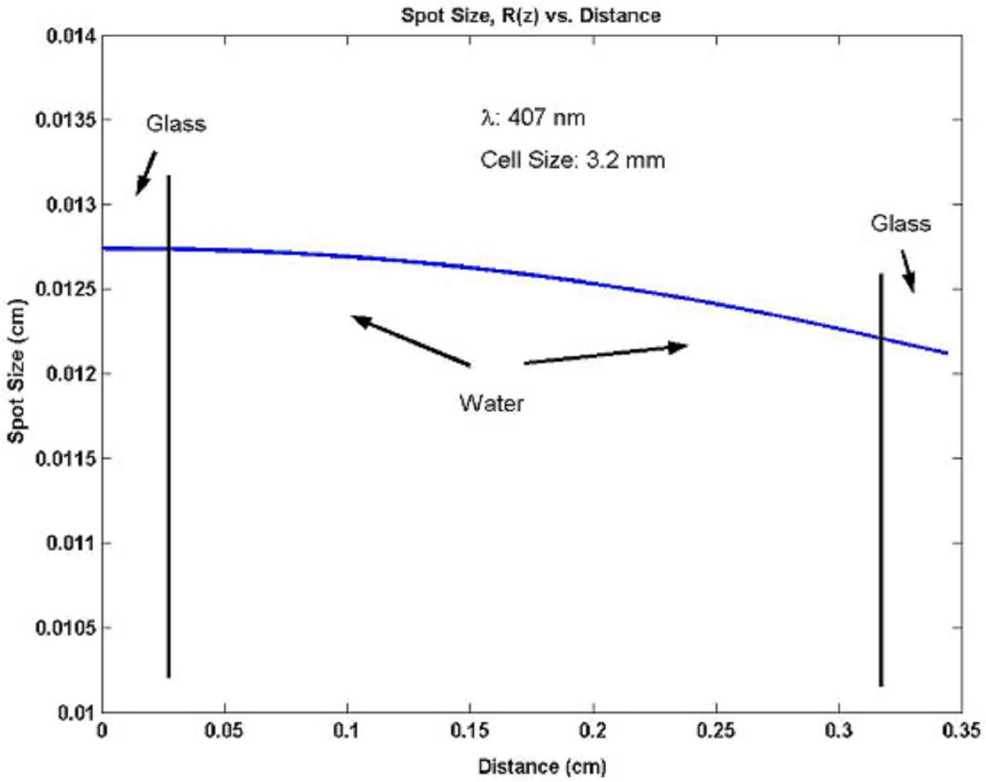

Figure 3.1: Simulation of the pulse radius R(z) as the blue 407 nm pump pulse travels through the fused silica windows (glass) and water cell. Energy of the pulse = 10 μJ with initial spot size 150 μm FWHM and initial pulse length FWHM 90 fs. Given those parameters the pulse compresses to 142 μm FWHM.

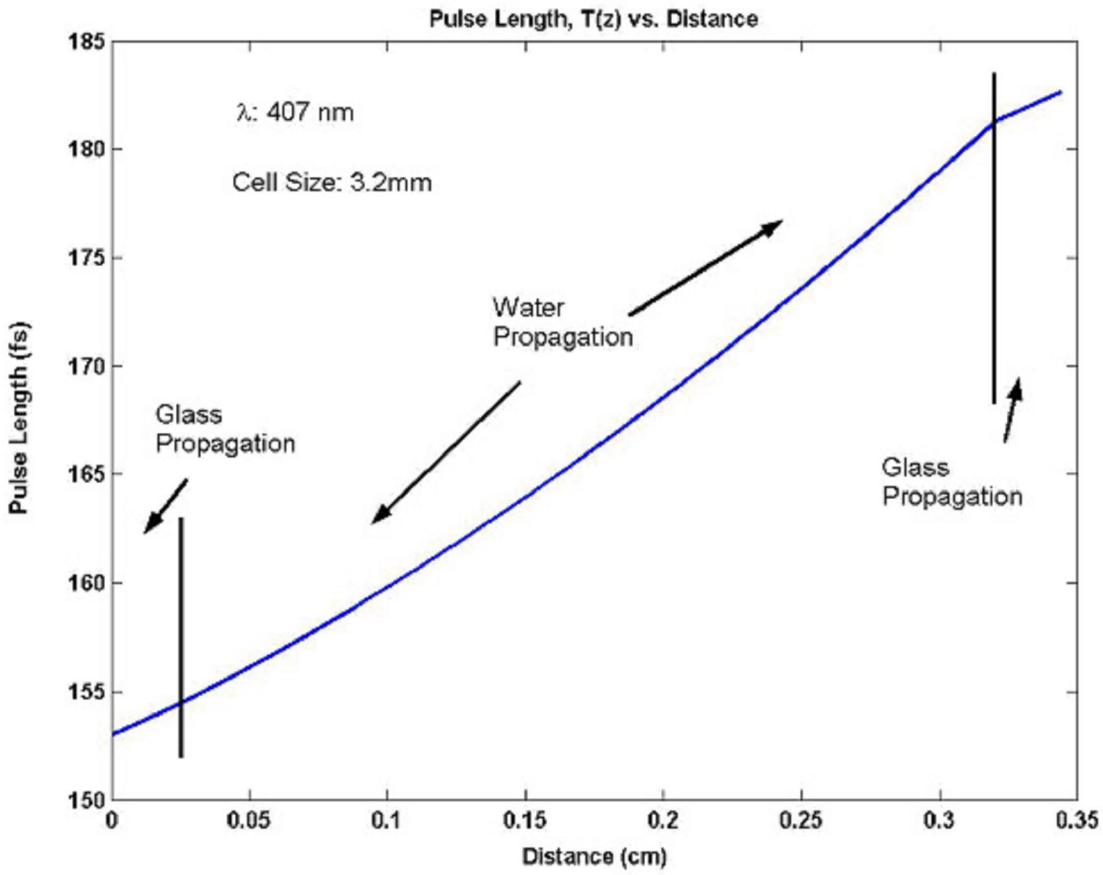

Figure 3.2: Simulation of the pulse length T(z) as the blue 407 nm pump pulse travels through the fused silica windows (glass) and water cell. Energy of the pulse = 10 mJ with initial spot size FWHM = 150 mm and initial pulse length FWHM 90 fs. Given those parameters the pulse broadens to 107 fs FWHM.

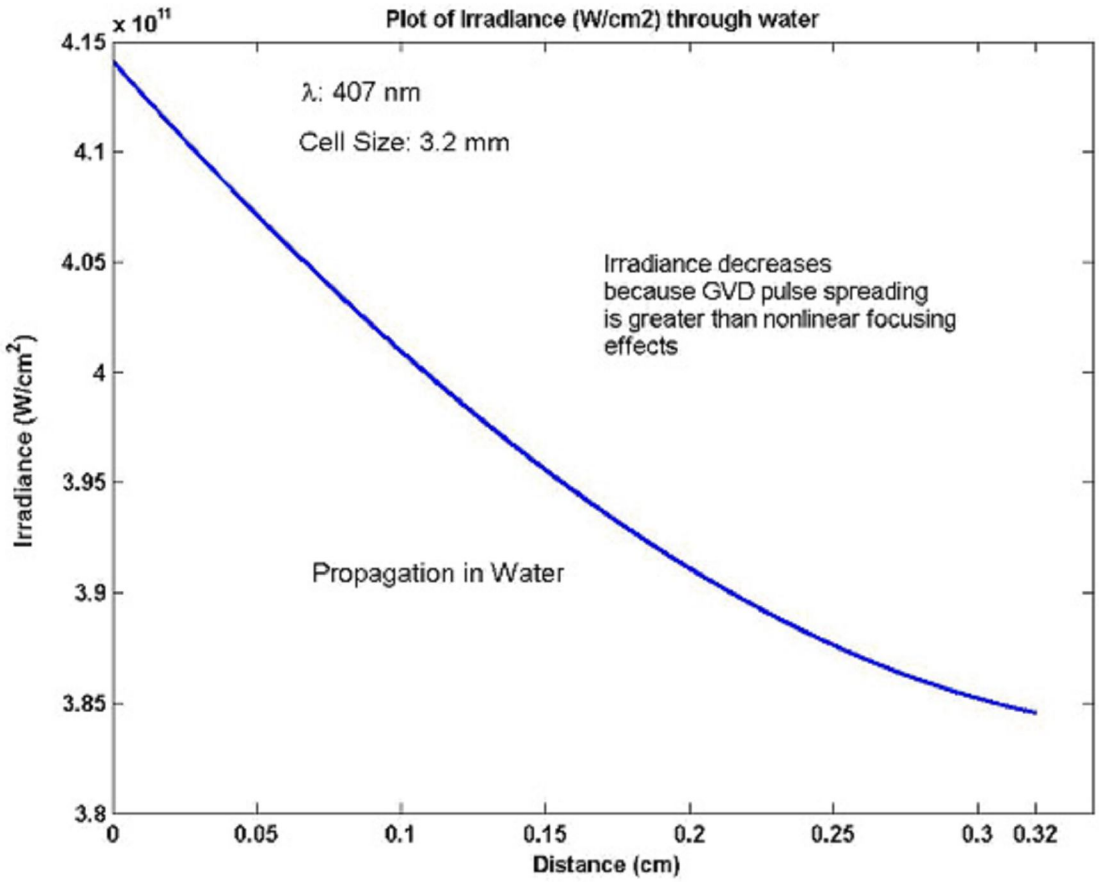

Figure 3.3: Simulation of the pump 407 nm pulse intensity through 3.2 mm of water accounting for nonlinear self-focusing and GVD broadening. GVD broadening dominates therefore decreasing pulse intensity. This is valid only for the simulation with E_o = 10 μJ, T(0) = 90 fs, initial spot size 150 μm FWHM.

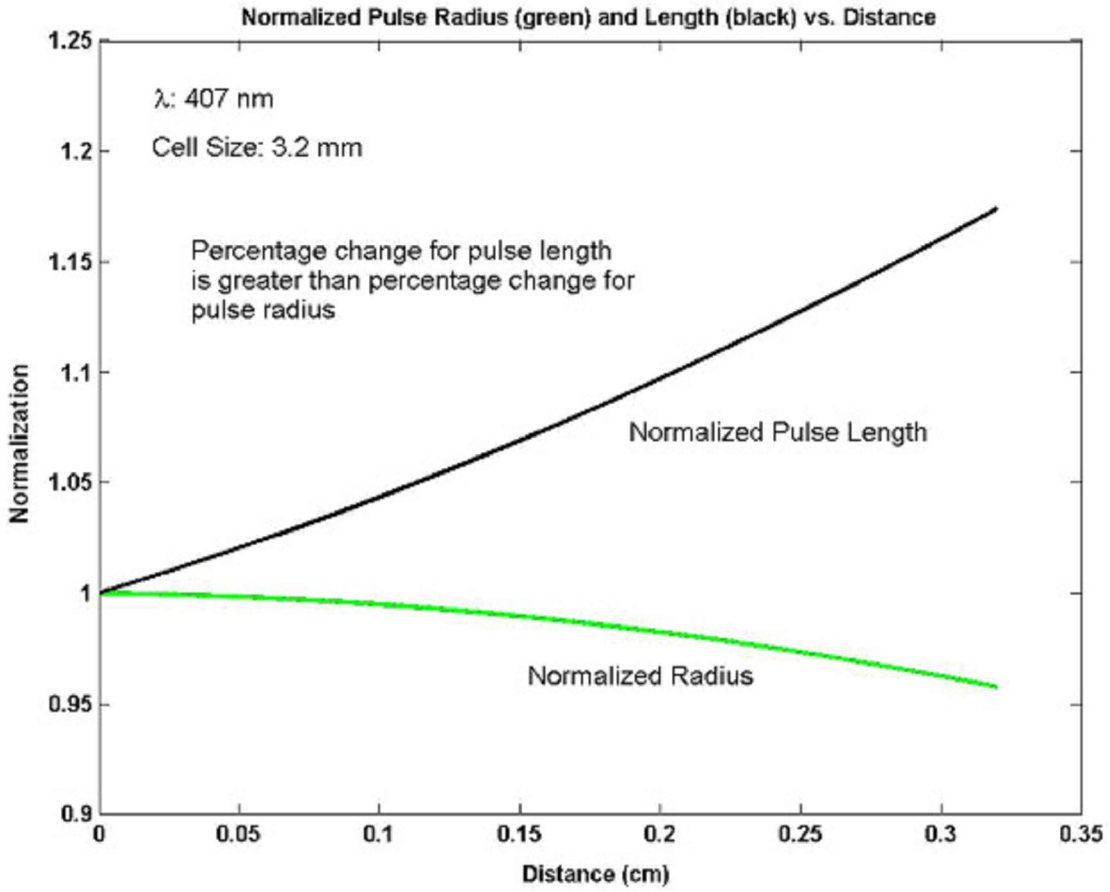

Figure 3.4: Normalized pulse radius R(z) and pulse length T(z) of the 407 nm pump pulse through a 3.2 mm water cell. The pulse broadening dominates self-focusing and therefore intensity decreases given the initial pulse parameters of E_o = 10 μJ, T(0) = 90 fs, initial spot size 150 μm FWHM.

Chapter 4: Experimental Setup

4.1 Setup

The process used to measure the nonlinear index of refraction is a process called single-shot supercontinuum spectral interferometry (SSSI). The setup involves a 1 mJ, 1 kilohertz, Ti:Sapphire Spitfire laser with pulse width 90 femtoseconds, measured with a home built GRENOUILLE[30], and central wavelength of 815 nanometers (see Appendix F for spectrum). The beam is split into two beams at beamsplitter 1 (BS1). One beam is used as the pump and the other for supercontinuum (SC) generation. Later, the pump will be frequency doubled with a 270 μm thick BBO (BBO) second-harmonic crystal with about 10% conversion efficiency (see Appendix F).

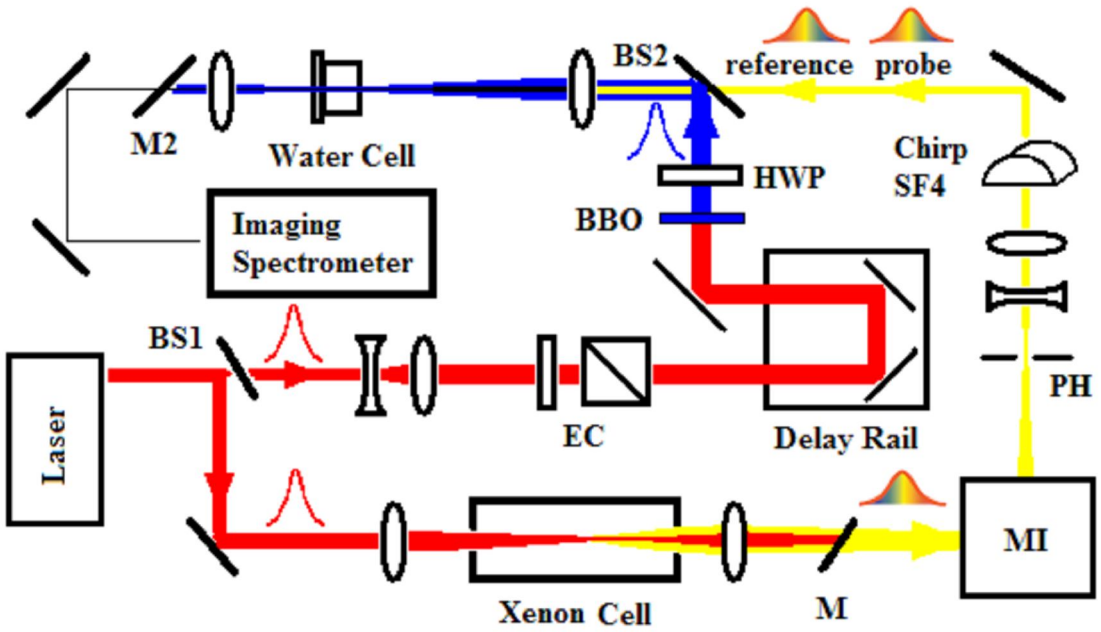

Figure 4.1: Experimental Setup for 407 nm Kerr index measurement. BS1, BS2: beamsplitters; MI: Michelson Interferometer; M, M2: pump beam dump mirrors; Chirp SF4: chirping crystal; PH: pinhole; BBO: SHG crystal; HWP: half waveplate used for relative polarization control; EC: energy control consisting of a half waveplate and cube polarizer.

The pump beam, consisting of the 90 femtosecond, 815-nanometer, and ~250 μJ, is sent to an adjustable delay line. This delay line allows the pump beam to be tuned in time relative to the SC beam. Before the delay line there is a half waveplate and polarizer pair that allows for energy control (EC) of the beam. After the delay line, a half waveplate (HWP) is used to provide independent polarization adjustment of the pump beam with respect to the SC[12]. By temporarily inserting a cube polarizer and monitoring the rejected beam the relative polarization of the pump was set.

The second beam, ~450 μJ and 90 femtoseconds long, propagates to an 11 centimeter long xenon cell (Xenon Cell) into which it is focused at f/6 in order to generate the ~100 nm width SC[12] centered around 690 nanometers. In generating the SC, the windows of the xenon cell were placed sufficiently far away from the beam filament/waist so as not to generate SC. When the SC along with the fundamental exit the xenon cell, the pulse is transversely chirped with frequency increasing radially[12]. Both fundamental and SC are then collected with an f/3 lens and converted into a weakly converging beam. This is then passed through a 0^{o}-800 nm high reflectivity mirror (M) to remove the fundamental. What is left is an approximately 10 μJ/pulse SC. The SC is then sent to a Michelson Interferometer (MI) in order to be split into twin reference and probe pulses. After the Michelson, the mildly converging beam becomes small enough so that a 500 μm pinhole (PH), capable of transverse fine tuning, is used to filter the SC to a high brightness, broad bandwidth, good spatial coherence, and smooth beam profile[12]. Beyond this the twin SC pulses are collimated with a 2x-magnifying telescope and sent through a 1-inch thick SF4 glass window (Chirp SF4) to be chirped. The result is twin SC pulses, 2 picoseconds apart in time (calculated from the wavelength difference

between fringes in the interferograms), positively chirped to 2 picoseconds, with a FWHM of 270 μm, a Rayleigh range of $z_{o,sc}$ = 24.6 cm., and a wavelength spread of 651 nanometers to 723 nanometers.

The pump beam and SC beam are combined at beamsplitter 2 (BS2) allowing for transmission of the supercontinuum and reflection at 45^o for the pump beam. Once combined the beams are then aligned so they propagate collinearly. The beams are then slightly focused using a 41 cm lens into the water cell. The delays are adjusted so the SC reference beam precedes the pump through the water cell, followed by the short pump pulse temporally and spatially superimposed on the SC probe. The Rayleigh range for the 815 nm pump was $z_{o,red}$ = 4.5 mm and $z_{o,blue}$ = 3.2 mm giving confocal parameters, $2z_o$, of 9.0 mm and 6.4 mm respectively.

The fused silica windows of the water cell were 240 μm thick so any contribution by the windows would be negligible. This was verified experimentally by draining the water from the cell and observing the phase shift, $\Delta\phi(\omega)$ between the reference and probe SC, of the fused silica windows on the imaging spectrometer due to cross-phase modulation between pump and probe. No recoverable $\Delta\phi(\omega)$ was found. A 270 μm probe beam overfills a smaller pump beam, ~30 μm FWHM for both red and blue pump pulses, transversely, allowing the whole transverse pulse interaction to be observed. The back plane, or exit, of the water cell interaction is then imaged on the imaging spectrometer slit at 6.9x magnification. Before arriving at the slit, either an 800 nm-0^o high reflectivity mirror or 400 nm-45^o mirror (M2) was used to dump the pump beam while the SC continued to the slit. The f/2 imaging spectrometer was composed of a diffraction grating with 1200 grooves per millimeter and a 10-bit camera capturing 7.5

fps at 1280x960 pixelation[12]. The spatial resolution of the CCD along the entrance slit direction was measured at 0.715 micron/pixel. The camera that captures the images is a SONY XCD-SX910 and is run using both a custom and out-of-the-box LabView program. The out-of-the-box program is used for alignment while the custom frame grabbing program, written by graduate student Andy York, is for a Firewire connection to a PC and allows for multiple shot data recording.

After replacing BS2 with a 45°-400nm mirror during the blue pump experiment, imaging of the SC was done before and after to verify that any adverse effects, like attenuation, did not manifest. The adverse effects were imperceptible above the normal SC energy and quality fluctuations.

4.2 Group Delay Dispersion

In order to extract the phase using the Fourier transform method outlined earlier, the group delay dispersion parameter, β_2, is needed. Using the method described in [16], and the equation[12] relating linear chirp coefficient to the GDD parameter, β_2, at the central frequency of a linearly chirped pulse, ω_o, and $\Delta\omega$ is the FWHM spectral width,

$$a = 2\beta_2\left(1 + (2\ln 2)^2 \beta_2^{-2} (\Delta\omega)^{-4}\right) \tag{4.1}$$

$$\beta_2 = \frac{1}{2}\frac{\partial^2\phi}{\partial\omega^2}\bigg|_{\omega o} \tag{4.2}$$

where a = linear chirp coefficient for a Gaussian pulse[13].

When determining the GDD parameter, cross-phase modulation, XPM, in a thin, 250 μm piece of fused silica was observed while incrementally scanning the delay of the pump relative to the probe and tracking the peak frequency ω_{peak} of the fringe shift, $\Delta\phi(\omega)$. The pump was delayed 11 times in 40.0 μm increments, corresponding to 133

femtosecond increments. Taking lineouts of the probe spectrum and knowing the wavelength to pixel mapping on the interferogram determined the spectral width, $\Delta\omega$, at FWHM of the SC. This gave a spectral width of 2.26×10^{14} rad/s. Wavelength to pixel mapping was calibrated using a neon lamp in the imaging spectrometer system.

From Figure 4.2, the linear chirp coefficient, 1.2×10^{11} rad*s^{-1}*fs^{-1}, was determined from the slope of the delay versus the frequency (wavelength) in the supercontinuum spectrum.

Because the supercontinuum spectral width is roughly 70 nm ($\Delta\omega = 2.26 \times 10^{14}$ rad/s), the factor $\beta^{-2}(\Delta\omega)^{-4}$ is << 1 leading to a GDD coefficient:

$$\begin{aligned} a &\cong 2\beta_2 \\ \beta_2 &= 4.17x10^3\ fs^2 \end{aligned} \tag{4.3}$$

4.3 Conclusion

The SSSI experimental setup consists of two beam lines one for pump and one for a supercontinuum consisting of a chirped probe and reference pulses. The probe pulse is modified by cross-phase modulation in the water cell and is interfered in an imaging spectrometer with an unmodified reference pulse. A student-developed MATLAB program is used to determine the phase shift due to cross-phase modulation in the probe beam by taking a Fourier transform of the interferogram images. From this phase shift information a nonlinear response can be calculated.

Modification of the setup to incorporate the 407 nm pump consisted of changing M2 to a 45^o-400nm mirror, BS2 to a 45^o-400nm mirror, adding a BBO crystal to produce 407 nm light, and inserting a filter (not shown) to remove 815 nm pump light from the beam path.

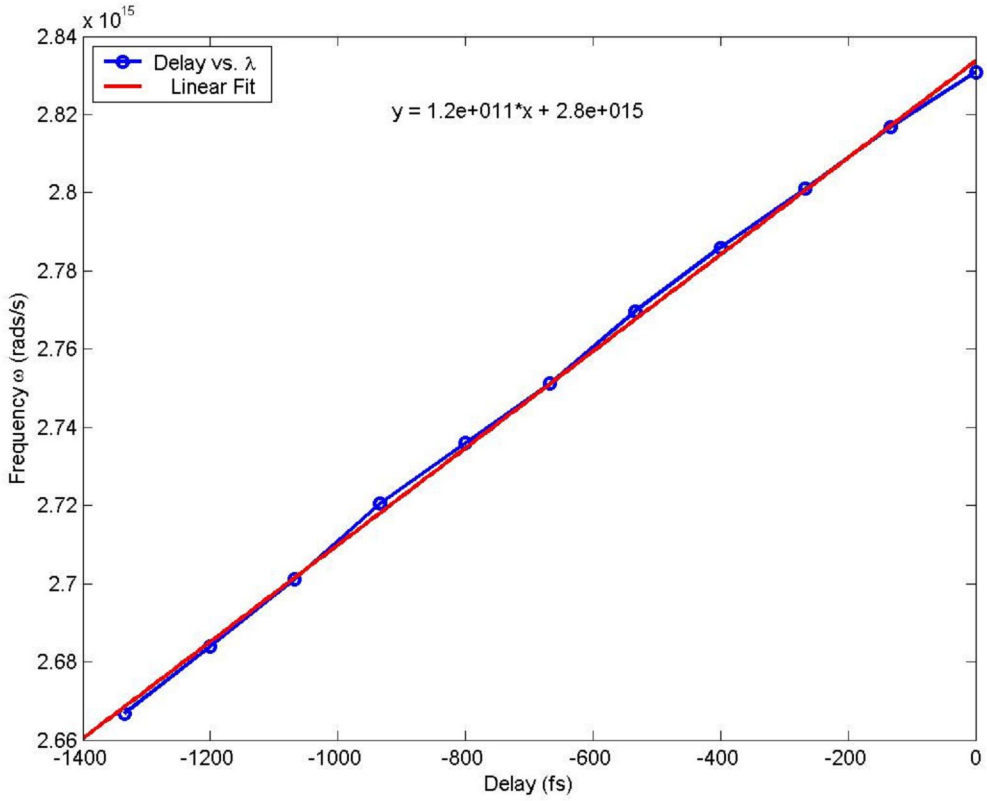

Figure 4.2: Plot of the delay (blue circles) with linear fit (red) versus frequency (wavelength) in determining the GDD parameter, β_2 of the SC used for SSSI.

Chapter 5: Results

5.1 Interferogram Acquisition

Figure 5.1 shows a) raw interferogram without the presence of the pump pulse and b) the interferogram with the pump pulse temporally overlapped with the SC probe.

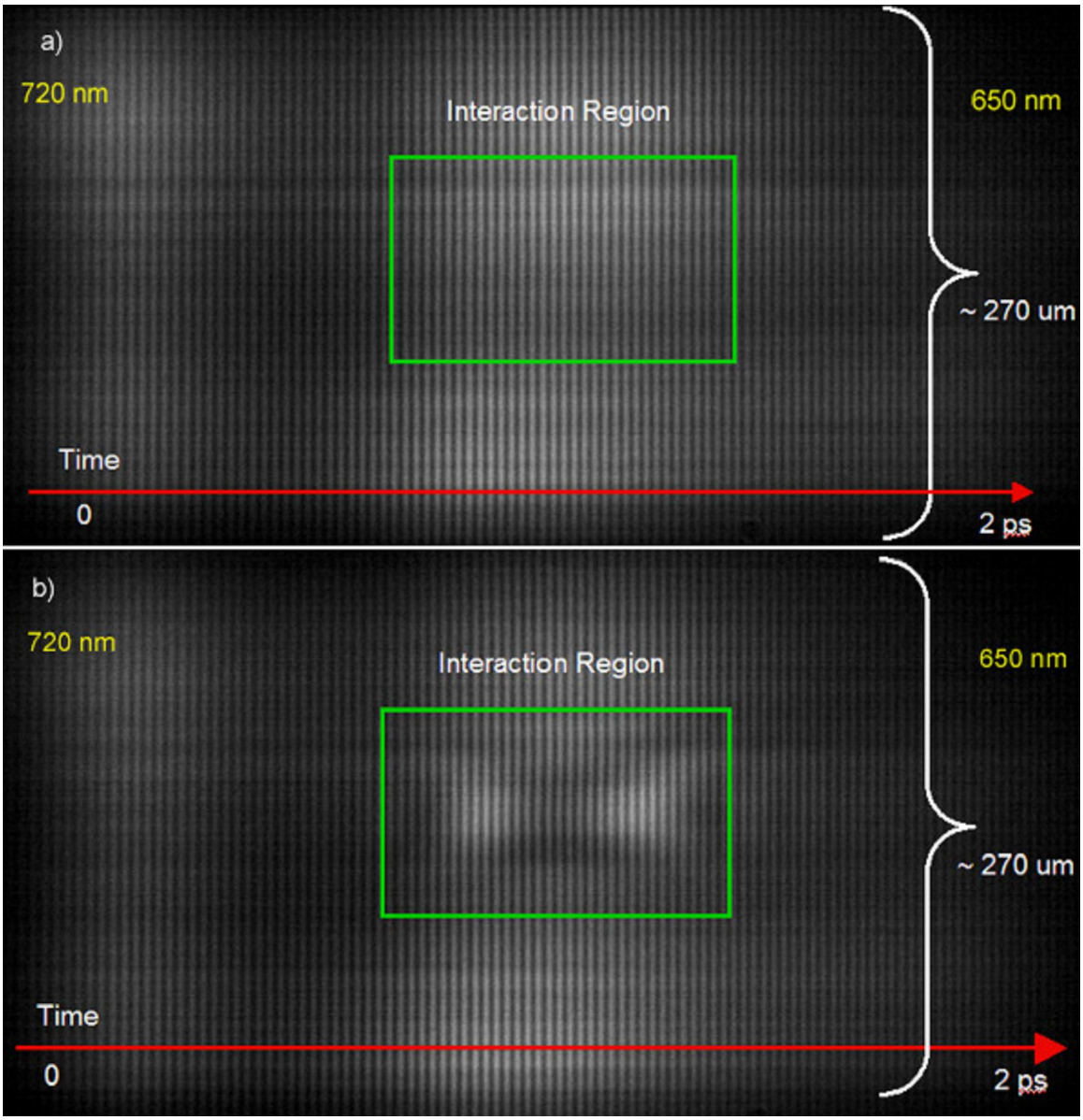

Figure 5.1: a) Raw interferogram without pump pulse phase shift showing transverse dimension of ~270 μm and a length of 2 picoseconds with ~720 nm light on the left and ~650 nanometer light on the right. b) Similar raw interferogram but with pump pulse introduced.

Figure 5.1a) represents what will be used as the background image and phase-shift information with 5.1b) representing the XPM phase shift. During the experiment, 300 images of each were taken and then averaged. Averaging was done to reduce the impact of shot-to-shot energy fluctuation and to remove background noise.

As discussed earlier the ionization intensity of water[3] at 815 nm and 45 fs was roughly 10^{13} W/cm^2. The peak intensity, I_o, of the pump for blue and red was kept far below this at ~$9x10^{10}$ W/cm^2. By keeping the intensity far from ionization plasma formation was prevented. Also, it was important that the self-focusing length[14] be kept greater than the pump's optical path through the water cell.

$$z_f = \frac{\pi w_o^2}{\lambda_o}\left(\frac{P}{P_{cr}} - 1\right)^{-1/2} \tag{5.1}$$

Each pulse intensity was ~ $9x10^{10}$ W/cm^2 and the beam sizes were w_o = 34 μm for the 815 nm pulse and w_o = 25 μm for the 407 nm. For the 815 nm pulse this corresponds to a peak power P = 3.3 MW. This is less than the critical self focusing power of 4.4 MW, from [19], and therefore focusing is determined by diffraction. For the blue pulse, the peak power is 1. 8 MW which is greater than the critical self focusing power of ~1 MW. This results in a self-focusing length of 4.2 mm which is greater than the largest optical path through the water cell of 3.2 mm. During the experiment no self-focusing was observed by examining pump spot images.

The effects of nonlinear self-focusing and pulse broadening (< 1% from group velocity dispersion, see Appendix H) are minimal over the interaction region thus allowing the nonlinear index of refraction to be extracted using Equation 1.22.

5.2 Red (815 nm) Nonlinear Index of Refraction

The nonlinear index of refraction value is obtained by considering the spatial peak phase shift, $\Delta\phi(x=0, t)_{peak}$, due to the peak intensity, $I(x=0, t)$. Figure 5.2 shows a lineout taken from Figure 5.7 with the red pump pulse, 815nm, with peak phase shift $\Delta\phi(x=0, t) = 1.26$ radians.

A Gaussian temporal profile is seen by the lineouts (Figures 5.3, 5.5) of the phase shift $\Delta\phi(x=0, t)$ through fused silica. The response in fused silica is electronic and therefore instantaneous as given by [21] thereby justifying a Gaussian shape temporal profile. Given a Gaussian temporal profile and the measured energy of the pulse, a peak power P_o is calculated. Using CCD images of the pump pulse spot the pixel values of the spot image are summed. This is done by selecting, via the MATLAB program (Appendix B), the region of interest, which is the spot image, and subtracting out the average background pixel value. Dividing the calculated peak power, P_o, by the pixel summation gives a peak power per digital pixel value conversion factor. Multiplying this conversion factor by the peak pixel value gives the peak power represented by the brightest pixel. Dividing this value by the pixel area gives peak intensity.

For the 815 nm pulse with FWHM 90 fs and an n_2 value was calculated to be:

$$n_{2\text{-red}} = 1.9\text{x}10^{-16} \pm 10\% \quad \text{cm}^2/\text{W}$$

where the error is due to the uncertainty in measured, not shot-to-shot, energy values. This value corresponds well with published data[3] and when used to calculate the critical nonlinear self-focusing power from the equation given by[3]:

$$P_{crit} = \frac{3.77\lambda^2}{8\pi n_o n_2} \tag{5.2}$$

P_{crit} = 4 MW. This agrees well with P_{crit} = 4.4 MW from [19].

It was necessary to check whether the nonlinear response was instantaneous. This was done by producing a phase plot of the shift in water, draining the water cell, increasing the energy so as to observe $\Delta\phi(x,t)$ in the fused silica windows and comparing the phase shifts $\Delta\phi(x=0,t)$. The method of draining the water introduced noise into the $\Delta\phi(x=0,t)_{fused\text{-}silica}$ plots because of tiny droplets left on the fused silica windows.

Figure 5.3 shows the overlay of the $\Delta\phi(x=0,t)_{fused\text{-}silica}$ versus $\Delta\phi(x=0,\ t)_{water}$. Because the fused silica phase shift is instantaneous, a purely electronic response[21] , it acts as a fiducial. When making the measurements it was noticed that the peaks between $\Delta\phi(x=0,t)_{fused\text{-}silica}$ and $\Delta\phi(x=0,\ t)_{water}$ were shifted in time by ~30 fs and ~50 fs (Fig. 5b)), relative to each other, depending on the thickness of the water cell. This comes from the "slipping" of the 815 nm light and SC λ_{center} = 690 nm group velocity mismatch.

In water the group velocity for the pump, λ = 815 nm, is greater than the group velocity for the SC λ_{center} = 690 nm which means one would expect to see $\Delta\phi(x=0,\ t)_{water}$ "ahead" in time relative to the $\Delta\phi(x=0,t)_{fused\text{-}silica}$. This is seen in Figure 5.5 where the $\Delta\phi(x=0,t)_{water}$ appears to be ahead in time relative to $\Delta\phi(x=0,t)_{fused\text{-}silica}$.

Looking at Figures 5.3 and 5.4 the group velocity mismatch is difficult to observe because the time resolution is approximately the same as the mismatch time, $t_{mismatch}$. The data-point-to-data-point resolution, t_{res} is ~25 fs determined by ~75 data points per 2ps window of time. Figures 5.5a,b depict the 815 nm, 90 fs pulse through the 3.2 mm water with and without $t_{mismatch}$ correction. When $t_{mismatch}$ is corrected, the $\Delta\phi(x=0,t)$ peaks for both fused silica and water align.

SSSI phase extraction of $\Delta\phi(x,\ t)$ shows the phase in both time and 1-D transverse

space. Figure 5.6 shows a 1-D transverse space and time $\Delta\phi(x, t)$ plot. No features or resurgent peaks appear in time after the pulse. Resurgent peaks would indicate molecular rotation. Without observing a shift between the $\Delta\phi(x=0,t)$ peaks of water and fused silica, without observing any pulse broadening between the $\Delta\phi(x=0,t)$ phase shifts of water and fused silica, and without observing features or resurgent peaks from the 1-D transverse space and time $\Delta\phi(x,t)$, the measured nonlinear response can be said to be the instantaneous electronic response.

During the experiment the linear polarization relative to the SC was varied from parallel to perpendicular. The perpendicular polarization relative to SC was tested in an attempt to observe a delayed molecular rotational response. However no conclusive data were observed.

Predicted earlier the factor between parallel and perpendicular should be 3. Figure 5.7 shows, for a parallel to SC polarized pump of 0.56 μJ and perpendicular to SC polarized pump of 0.63 μJ, a peak phase shift ratio $\Delta\phi(x=0,t)_{parallel}/\Delta\phi(x=0,t)_{perpendicular}$ = 3.3. This agrees with predicted behavior of parallel and perpendicular to SC polarization when an XPM $\Delta\phi(x=0, t)$ is measured.

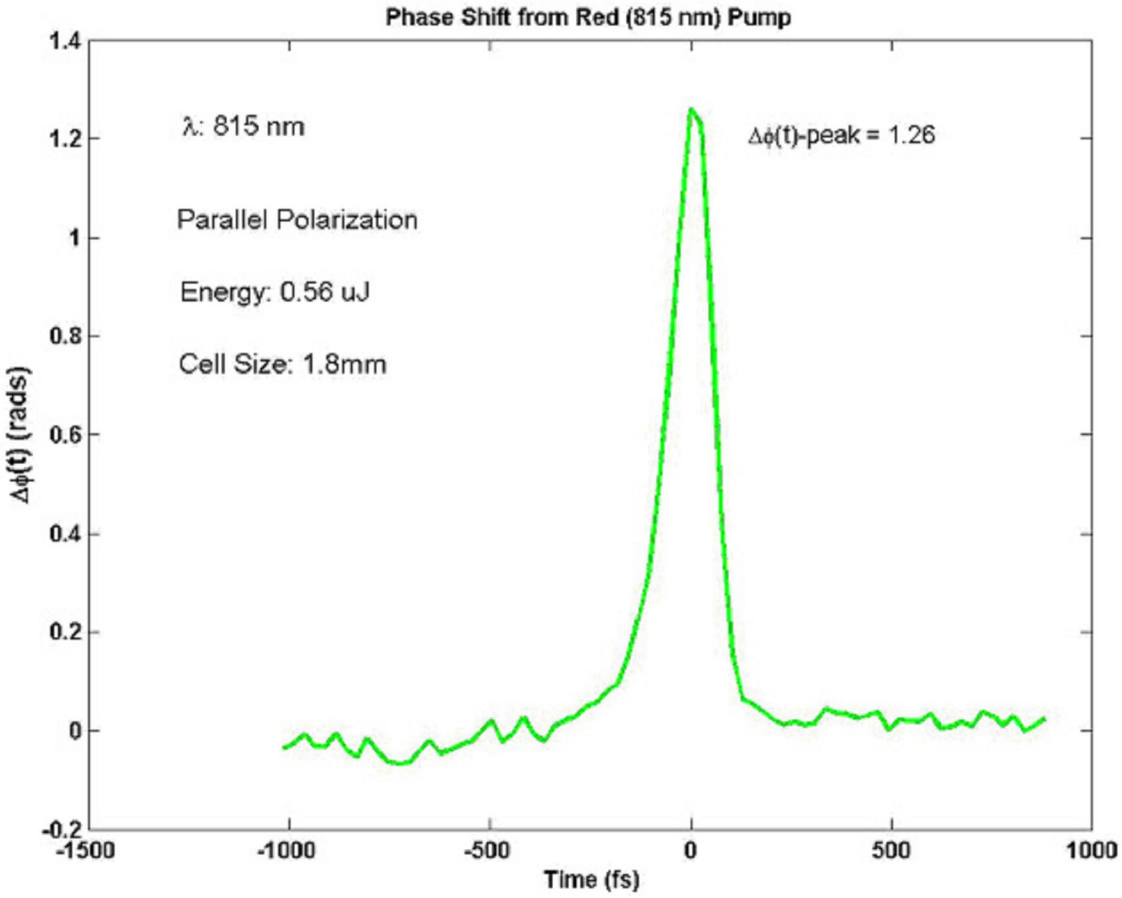

Figure 5.2: 300 shot average (green line) of phase shift $\Delta\phi(x=0,t)$ along the axis of an 815 nm pump pulse of 0.56 μJ with $I_{peak} = 1.9 \times 10^{11}$ W/cm^2 through 3.2 mm of doubly distilled water. The $n_{2\text{-water}}$ value obtained for 815 nm light agrees well with other published data.

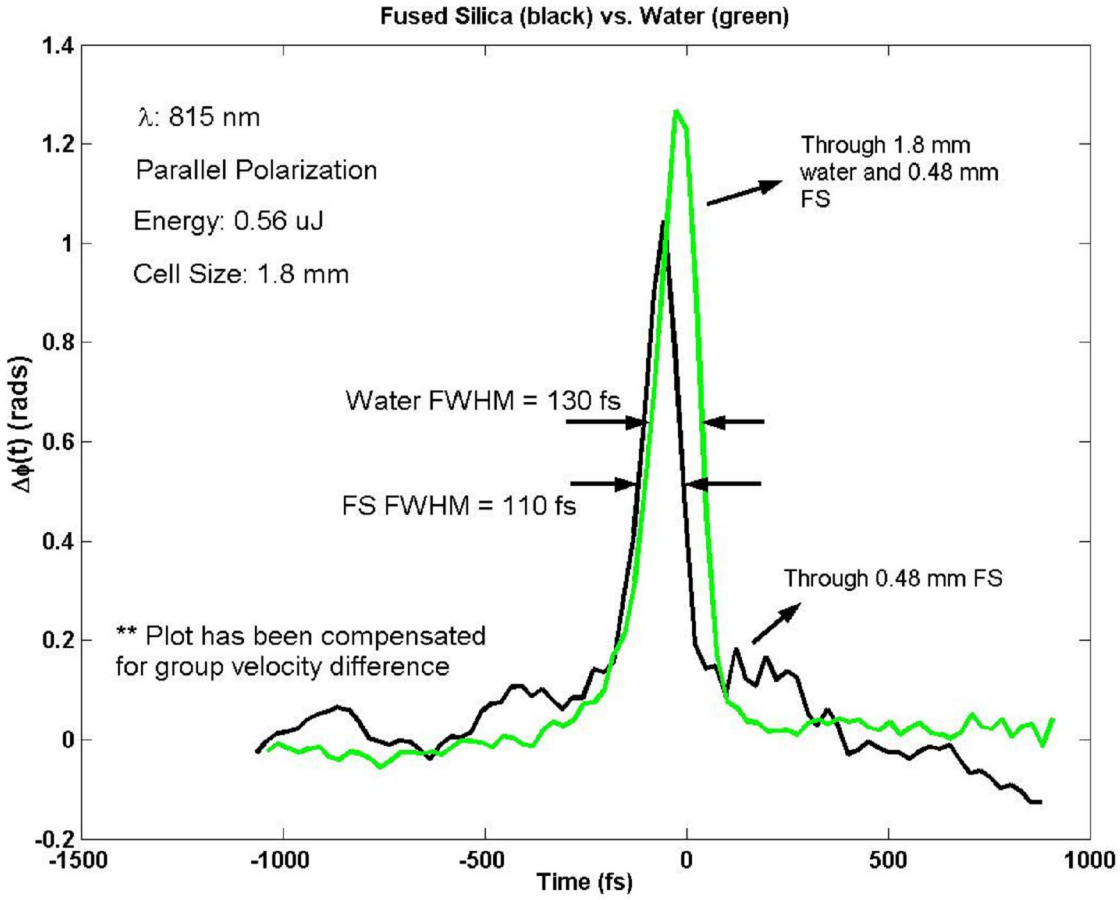

Figure 5.3: 300 shot average of phase shift $\Delta\phi(x=0,t)$ along the axis of an 815 nm pump pulse of 0.56 μJ through a 1.8 mm thick water cell (green) and of a ~5uJ pulse through 0.48 mm of fused silica (black). The fused silica serves as a measure of instantaneous n_2. Within the time resolution ~25 fs, the pulses in water and fused silica have the same FWHM pulse length indicating an instantaneous n_2 response of water at 815 nm when $t_{mismatch}$ of ~50 fs has been corrected.

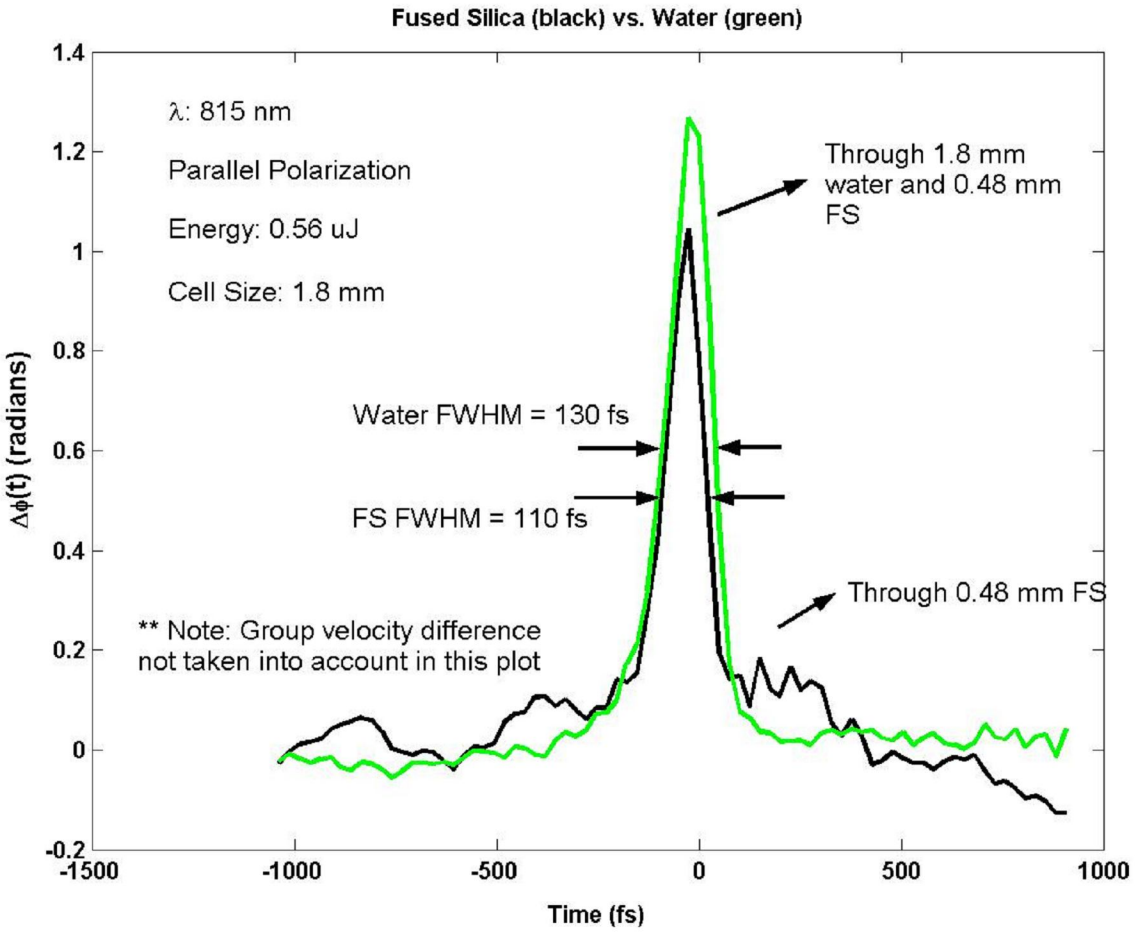

Figure 5.4: 300 shot average of phase shift $\Delta\phi(x=0,t)$ along the axis of an 815 nm pump pulse of 0.56 μJ through a 1.8 mm thick water cell (green) and of a ~5uJ pulse through 0.48 mm of fused silica (black) to serve as a measure of instantaneous n_2. Group velocity mismatch of ~30 fs has not been accounted for.

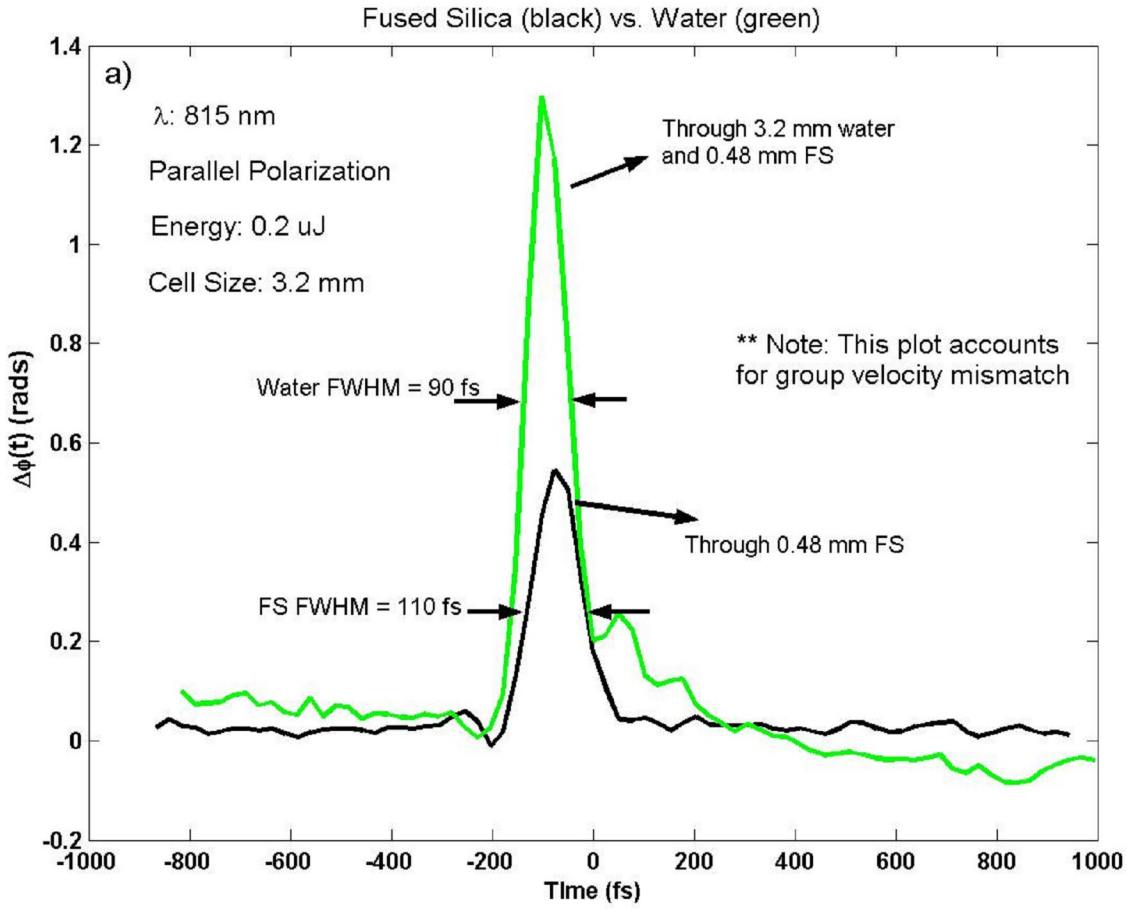

Figure 5.5-a) 300 shot average of phase shift $\Delta\phi(x=0,t)$ along the axis of an 815 nm pump pulse of 0.2 μJ through a 3.2 mm thick water cell (green) and of a ~5uJ pulse through 0.48 mm of fused silica (black). The fused silica serves as a measure of instantaneous n_2. Within the time resolution ~25 fs, the pulses in water and fused silica have the same FWHM pulse length indicating a purely instantaneous n_2 response of water at 815 nm when $t_{mismatch}$ of ~50 fs has been corrected.

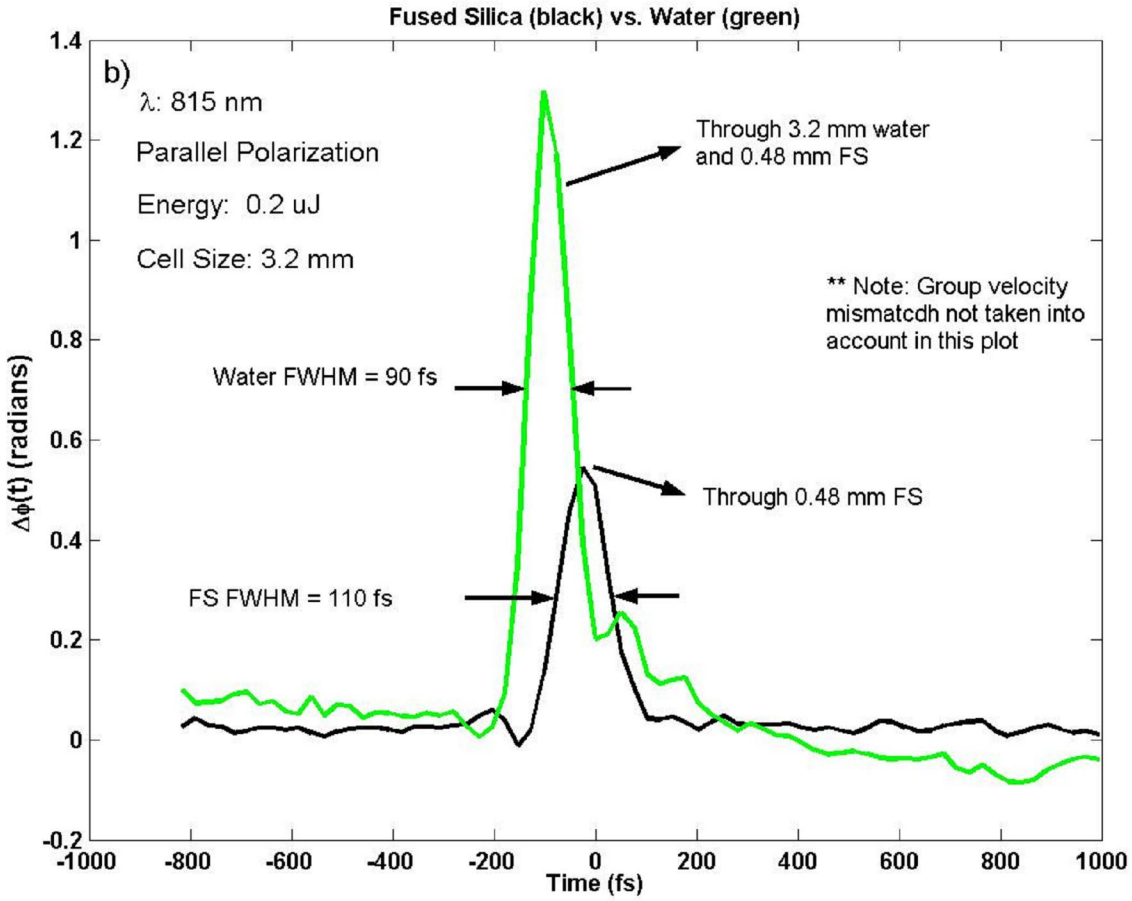

Figure 5.5-b) Similar to **a)** but $t_{mismatch}$ has not been corrected. Pulse appears to be "ahead" in time.

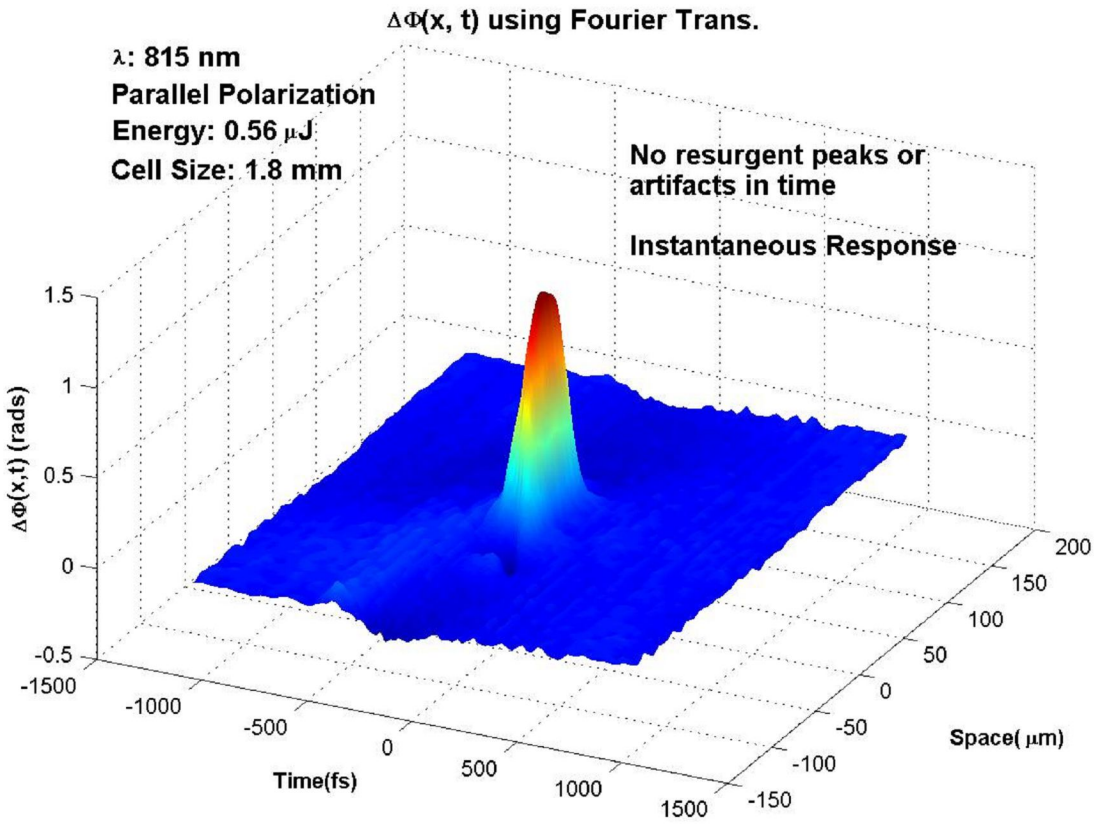

Figure 5.6: 300 shot average of $\Delta\phi(x, t)$ in time and 1-D transverse space of a 0.56 μJ pulse with I_{peak} = 1.9x10^{11} W/cm^2 through 1.8 mm water cell. No resurgent pulses (rotational revivals[22]) and no artifacts therefore $n_{2\text{-red}}$ is an instantaneous response at 815 nm, 90 fs FWHM.

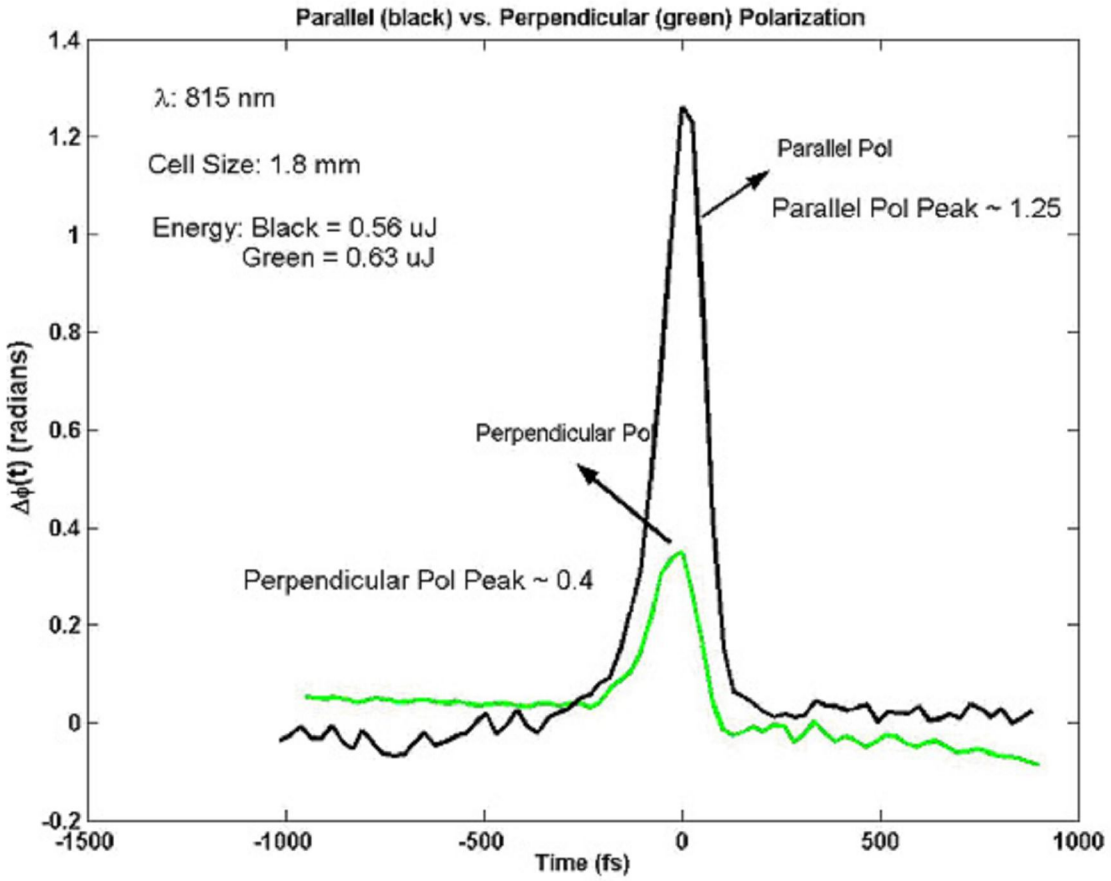

Figure 5.7: 300 shot average of both parallel (black) and perpendicular (green) polarization relative to the SC where $\Delta\phi(x=0,t)_{parallel}/\Delta\phi(x=0,t)_{perpendicular} = 3.3$ which is in agreement with theory of linearly cross polarized XPM. Times are arbitrary between plots.

5.3 Blue (407 nm) Nonlinear Index of Refraction

Much like the 815 nm pump pulse determination of n_2, a value for n_2 at 407 nm was measured. When extracting $\Delta\phi(x, t)_{blue}$ a feature on the leading edge in time kept surfacing. This remains unexplained at this point.

Beginning with the effective $\Delta n(x,t)$ extraction, the setup was modified to produce a λ_{center} = 407 nm pump pulse. The pulse length for 407 nm could not be measured with GRENOUILLE like the 815 nm pump, so was therefore measured using the $\Delta\phi(x=0, t)$ in fused silica. Fused silica n_2 response is electronic and therefore taken to be instantaneous[21] providing a mapping of the pulse duration and 1-D space profile. From this the pulse duration was determined to be ~250 fs FWHM and approximately Gaussian.

The measurement of the nonlinear index of refraction was achieved through the SSSI pump-probe configuration. The 400 nm pump pulse induces the nonlinear response from the water and alters its index of refraction. The probe pulse is weak enough itself not to cause further modification of the refractive index. It only samples the newly changed index of refraction and results in a linear phase shift proportional to the induced nonlinear change in the refractive index. The exact wavelength of the probe pulse only comes in as far as dispersion is concerned. If neither the pump wavelength nor the probe wavelength is close to an electronic resonance in the media, the wavelength dependence on the probe radiation should be minimal. A comparison with a situation where the pump acts as its own probe requires further consideration. Even in the case where the probe frequency is equal to the pump frequency, the degeneracy factor is still 2[7].

Figure 5.8 shows a $\Delta\phi(x=0, t)$ lineout taken of the blue pump pulse, λ = 407 nm with an on axis peak phase shift of $\Delta\phi(x=0, t)_{peak}$ = 1.17 radians, energy of 0.6 μJ, I_{peak} = $9.5x10^{10}$ W/cm^2, and pulse length of ~250 fs FWHM. The value below represents an effective nonlinear index of refraction which a 400 nm pulse would experience as self-phase modulation. By modifying the code in Appendix B an effective $n_{2\text{-blue}}$ was found:

$$n_{2\text{-blue}} = 1.7x10^{-16} \pm 12\% \quad cm^2/W$$

where the error is due to measurement uncertainty in pulse energy, not shot-to-shot energy fluctuation. Also, the calculated value was the same for both water cell thicknesses suggesting that any group velocity mismatch between pump and probe did not affect the measurement.

The calculated value suggests a critical self-focusing power of P_{crit} = 1.1 MW which is consistent with previously published values for similar wavelengths and a range of pulse durations.

As previously stated the pump was propagated in fused silica to obtain a fiducial and like the 815 nm experiments, the $\Delta\phi(x=0, t)$ plots revealed large Δt between the $\Delta\phi(x=0, t)_{fused\text{-}silica}$ and $\Delta\phi(x=0, t)_{water}$ peaks. The group velocity mismatch between the pump 407 nm and SC λ_{center} = 690 nm was ~200 fs and ~370 fs for the 1.8 mm and 3.2 mm water cells respectively. Unlike the red 815 nm pump, the blue 407nm pump will appear to "fall behind" in time from the pulse in fused silica because the group velocity, v_g of 407 nm is less than v_g of 690 nm in water.

Figure 5.9 depicts the blue pump through both fused silica and 1.8 mm of water without compensation for $t_{mismatch}$. It shows a $\Delta\phi(x=0, t)_{water}$ trailing a fused silica $\Delta\phi(x=0, t)_{fused\text{-}silica}$ and when corrected, Figure 5.10, the $\Delta\phi(x=0, t)$ peaks match up.

Interestingly the leading edge feature does not appear to be a pulse broadening effect since the pulse width remains the same, ~250 fs FWHM. For the $\Delta\phi(x=0, t)$ lineouts there are ~75 data points per 2ps window of time giving a data point to data point resolution of ~25 fs.

In an attempt to understand the leading edge feature, it is necessary to look at the 1-D transverse and time plot $\Delta\phi(x, t)$. In Figure 5.11 a parallel polarized relative to SC pulse, energy of 0.6 μJ, ~250 FWHM pulse length, through a 3.2 mm water cell, I_{peak} = $9.5x10^{10}$ W/cm^2 clearly depicts a "ridge" on the leading edge. This "ridge" is observed to last 100-200 fs ending at approximately half of the $\Delta\phi(x=0, t)$ peak.

A possible model and explanation for the ridge feature comes from [23] which suggest several nonlinear susceptibility phenomena that occur in simple liquids (e.g. CS_2) which include an ultrafast damping ($\tau_{1/e}$ <170 fs) associated with molecular librational motion (a "rocking" rotation of molecules within an intermolecular potential in which the molecules must move[23]) and an intermolecular "interaction-induced" distortion of the molecular polarizability with $\tau_{1/e}$ ~ 400-600 fs. This is the changing of the molecular polarizability due to the intermolecular translation and rotational collisions.

Another paper [24] indicates, by observing transient optical Kerr effects in CS_2, the artifact may be the result of the intramolecular instantaneous electronic response, E_{inst}, and intermolecular dynamics. The paper makes use of an inertial Debye dephasing inhomogeneous oscillator model. This model contains terms describing three separate intermolecular dynamics: molecular reorientation – Γ_D from the diffusion equation of motion, molecular redistribution – Γ_T which arises from mutual interaction between the dipoles induced in the medium molecules by strong incident fields[24], and molecular

libration – L which occurs as the molecule is torqued and released momentarily by the incident electric field[24]. From the paper the fastest is L, then Γ_T, and the slowest is Γ_D but the lifetimes are to be determined by fitting experimental data[24]. From the paper, the dominating dynamics are E_{inst} and L and when the laser pulse is sufficiently short, the two responses are separate and observable (Figure 5.12a). When the pulse is lengthened, the instantaneous and librational responses overlap and a ridge appears (Figure 5.12b).

For completeness, Figure 5.13 shows the effect of parallel and perpendicular polarization relative to the SC by the 407 nm pump pulse. Again, the peak phase shift ratio $\Delta\phi(x=0,t)_{parallel}/\Delta\phi(x=0,t)_{perpendicular} = 3.3$. Since the time dependence of the phase-shift is observable, the correlation to an instantaneous theory factor of 3 cannot be asserted. Both parallel (Fig. 5.13 black line) and perpendicular (Fig. 5.13 green line) exhibit a ridge of ~ 200 fs on the leading edge.

5.4 Conclusion

From the data the value for the nonlinear index of refraction of water due to 815 nm light was found to be $n_2 = 1.9 \times 10^{-16}$ cm^2/W +/-10% with no delayed response observed. From the data an effective nonlinear response of water at 407 nm was calculated to be 1.7×10^{-16} cm^2/W +/-12%. Observed in the phase-shift data from the cross-phase modulation of the 407 nm pump with the ~690nm supercontinuum was a ridge feature. This feature could indicate a delayed response which may have origins in intermolecular libration of the water molecules. Further studies would have to be done to confirm this hypothesis.

Changing the relative polarization between pump and probe pulses did not provide any new information about delayed responses, however the data did show for the 815 nm pump a factor of 3 when compared with parallel relative polarization. This is consistent with theoretical calculations.

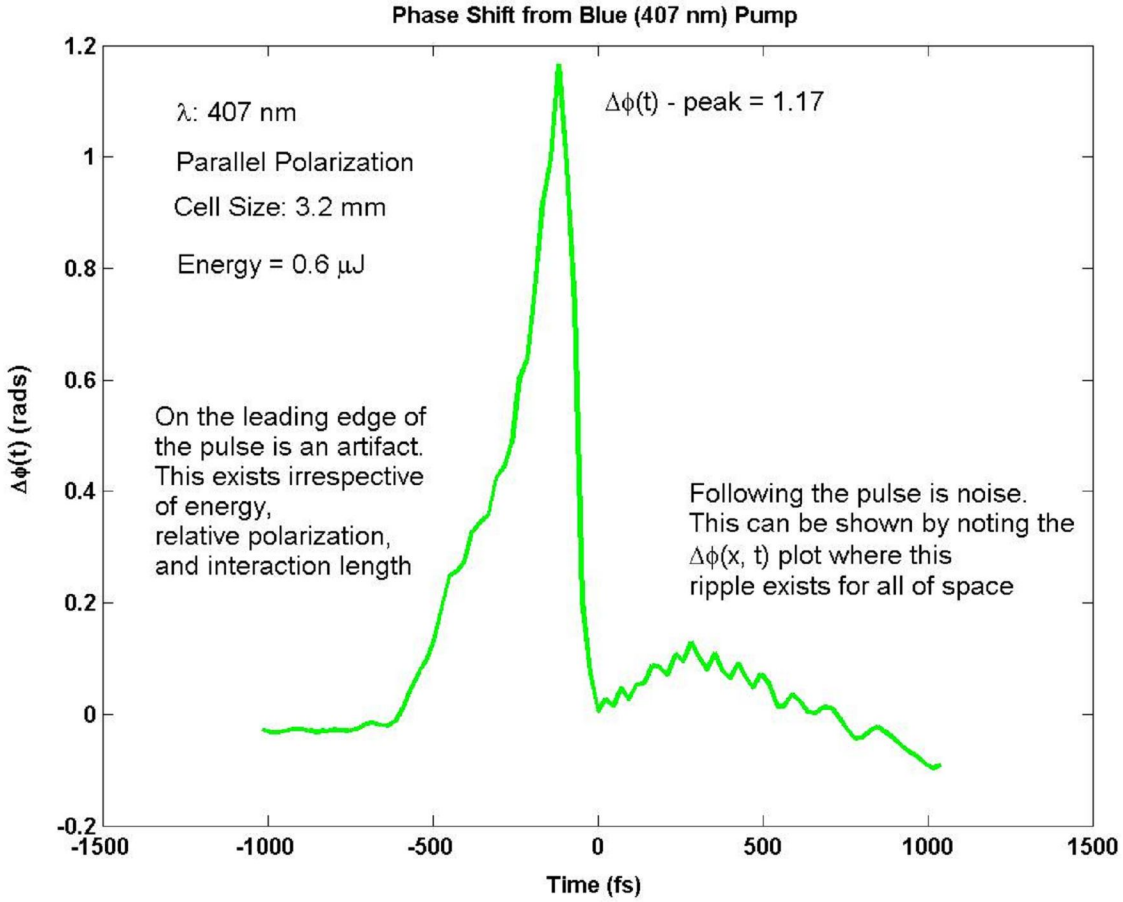

Figure 5.8: 300 shot average of a 407 nm pump pulse, 0.6 μJ, ~250 fs FWHM pulse length, I_{peak} = 9.5x10^{10} W/cm^2, in a 3.2 mm water cell. The instantaneous $n_{2\text{-blue}}$ when used to calculate P_{crit} agrees with an NRL experimental value. This lineout shows a leading edge artifact independent of pulse energy, interaction length, and relative polarization.

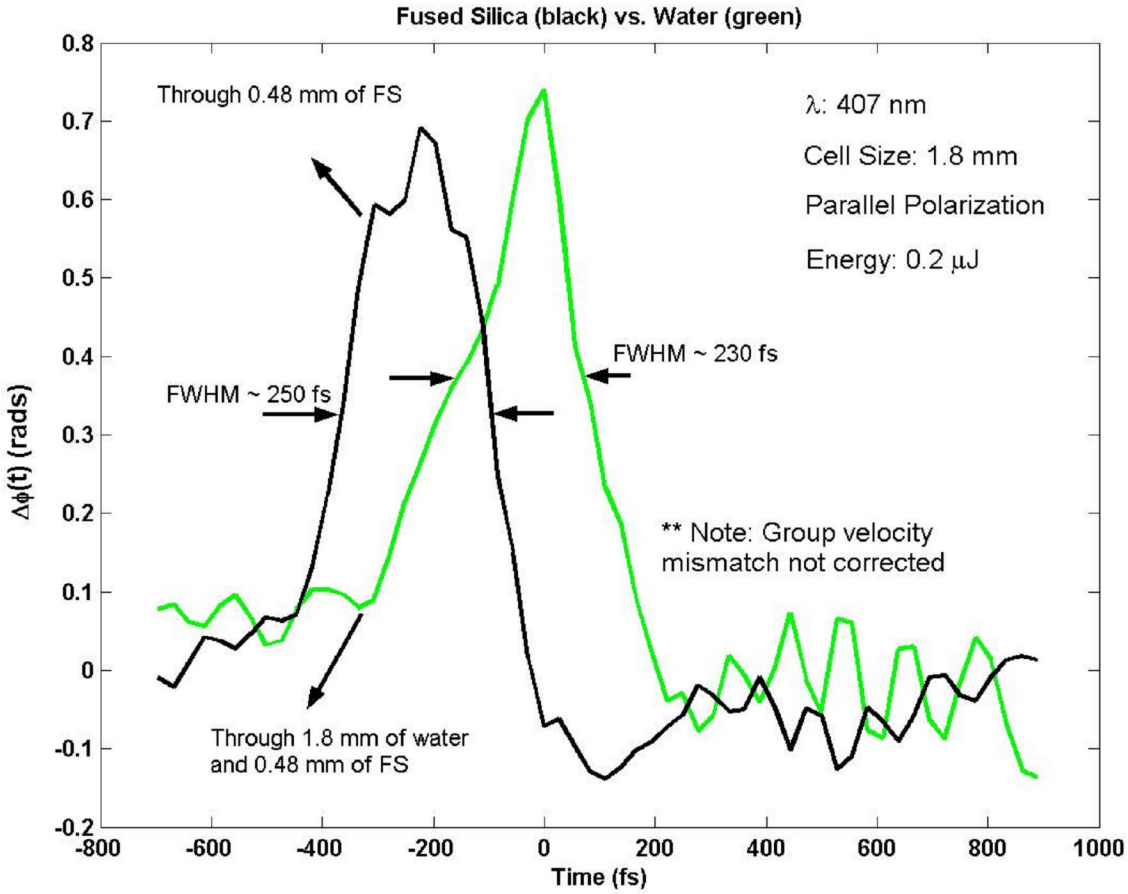

Figure 5.9: 300 shot average of $\Delta\phi(x=0, t)$ along the axis of 407 nm pump in 1.8 mm water (green) and in fused silica (black) in order to relate time dependent $\Delta n_2(t)$. The $\Delta\phi(x=0,t)_{water}$ with energy 0.2 μJ, ~250 fs FWHM pulse length, $I_{peak} = 1.3x10^{11}$ W/cm^2 appears delayed in time however $t_{mismatch}$ ~200 fs has not been corrected. The green plot contains the leading edge artifact and ripple noise on the trailing tail. Small peaks and trailing ripple artifacts in the fused silica $\Delta\phi(x=0, t)$ are due to noise.

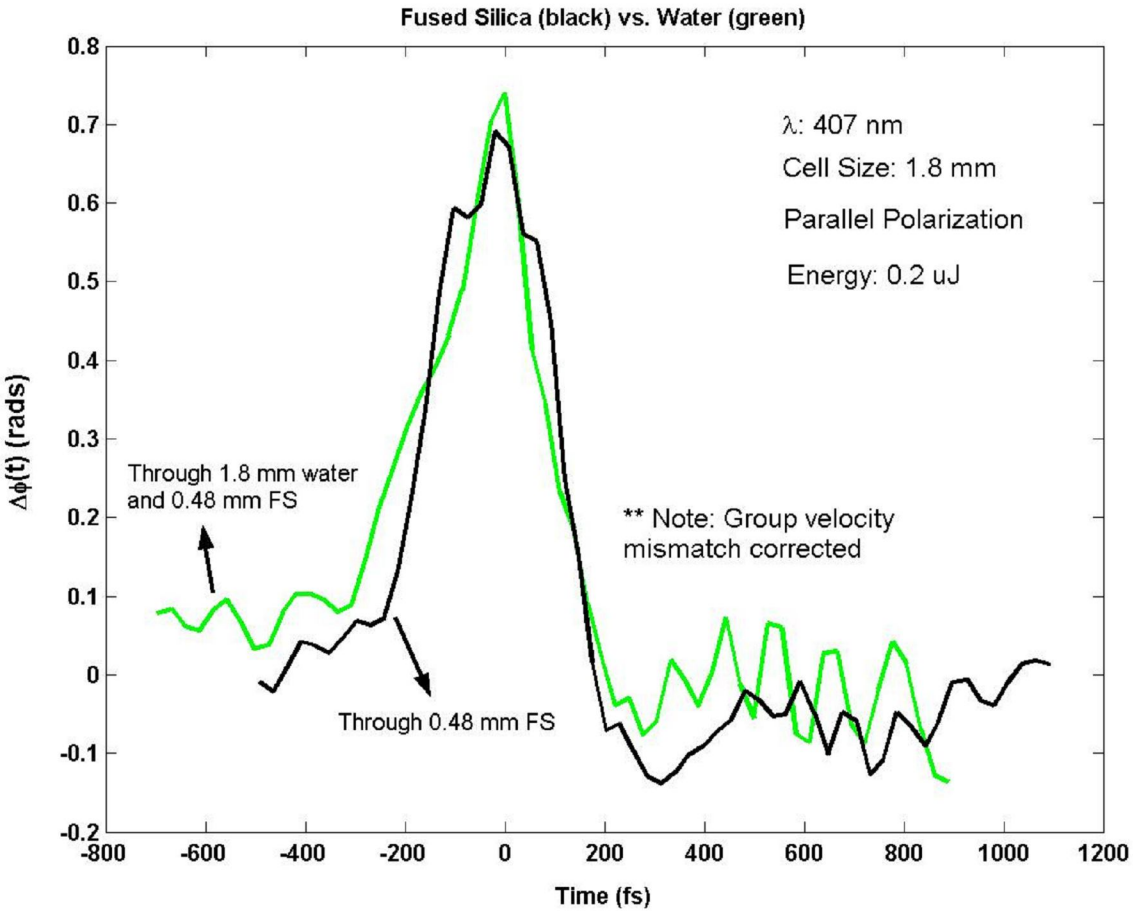

Figure 5.10: 300 shot average of $\Delta\phi(x=0, t)$ along the axis of 407 nm pump in 1.8 mm water (green) and in fused silica (black) in order to relate time dependent $\Delta n_2(t)$. The $\Delta\phi(x=0,t)_{water}$ with energy 0.2 μJ, ~250 fs FWHM pulse length, $I_{peak} = 1.3x10^{11}$ W/cm^2 overlapped in time with the $\Delta\phi(x=0, t)_{fused\text{-}silica}$ plot when the $t_{mismatch}$ ~200 fs is corrected. The green plot contains the leading edge artifact and ripple noise on the trailing tail. Small peaks and trailing ripple artifacts in the fused silica $\Delta\phi(x=0, t)$ are due to noise.

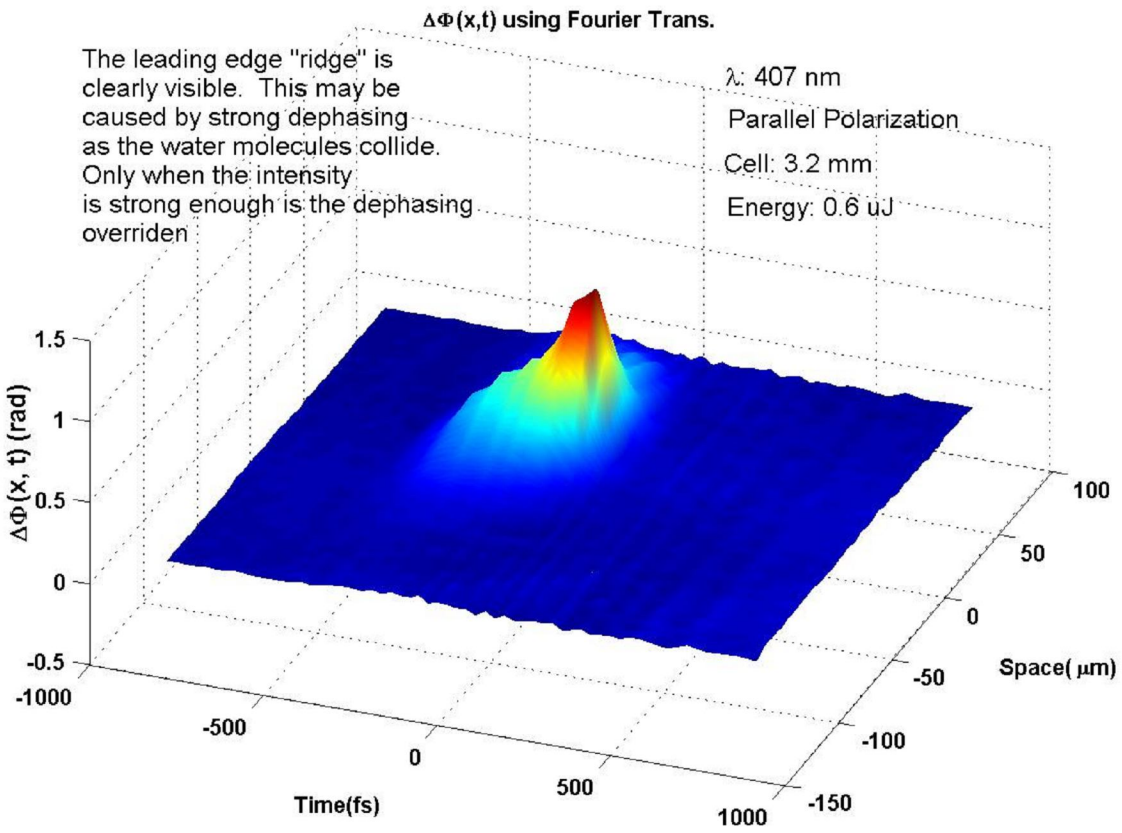

Figure 5.11: 300 shot average of the phase shift $\Delta\phi(x, t)$ from a 0.6 μJ, ~250 fs FWHM, 407 nm pump pulse showing an approximate Gaussian spatial profile, $\Delta\phi(x)$ with a leading edge "ridge". The "ridge" exists for ~200 fs.

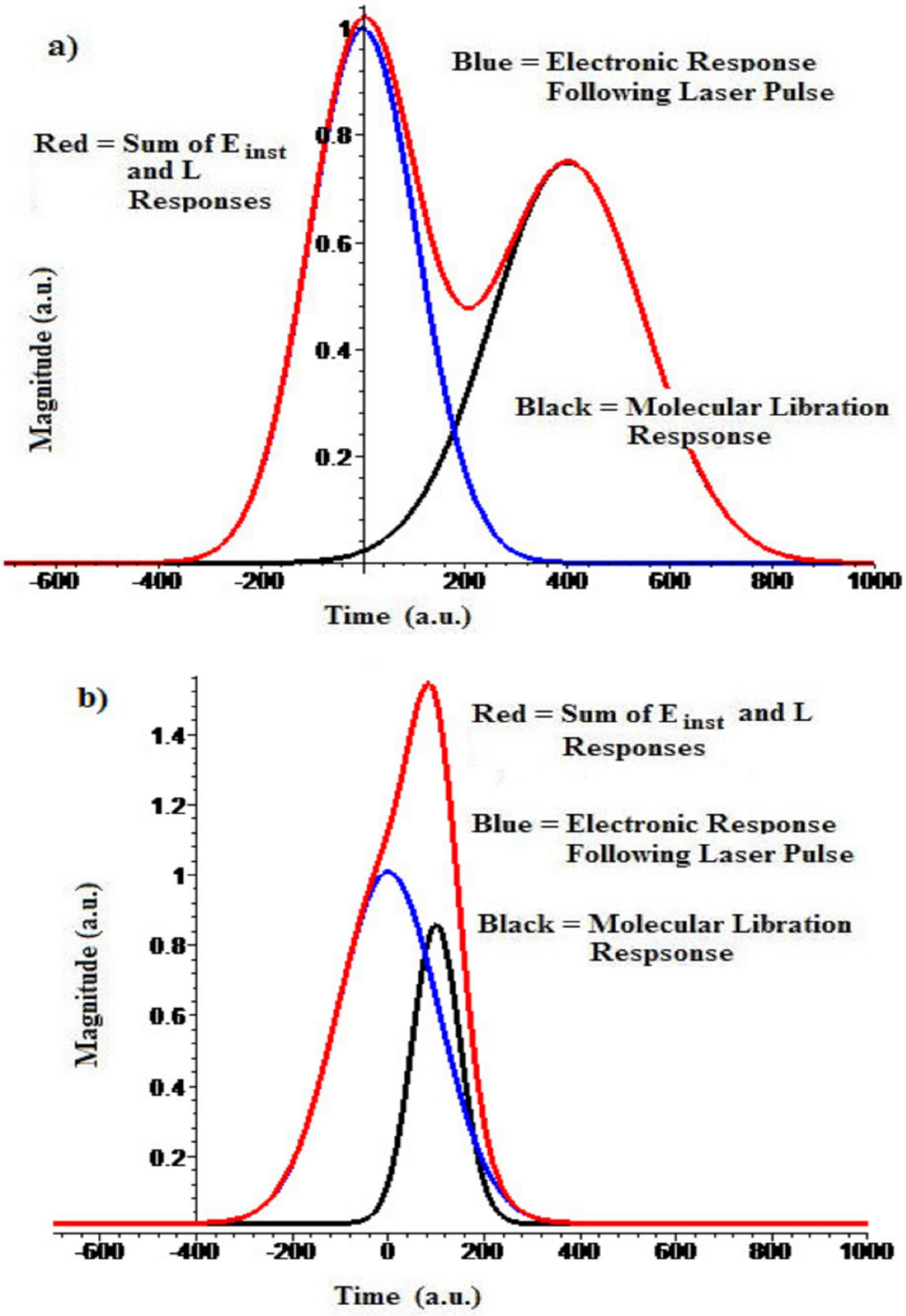

Figures 5.12a, b: Theoretical plots of instantaneous electronic response, E_{inst}, and librational response, L, for liquid H_2O. **a)** Double peak (red) $\Delta\phi(x=0, t)$ response when an ultrafast pulse envelope (blue) interaction outpaces librational response (black). **b) "**Ridge" $\Delta\phi(x=0, t)$ response (red) when an ultrafast pulse envelope (blue) interaction and librational response (black) overlap.

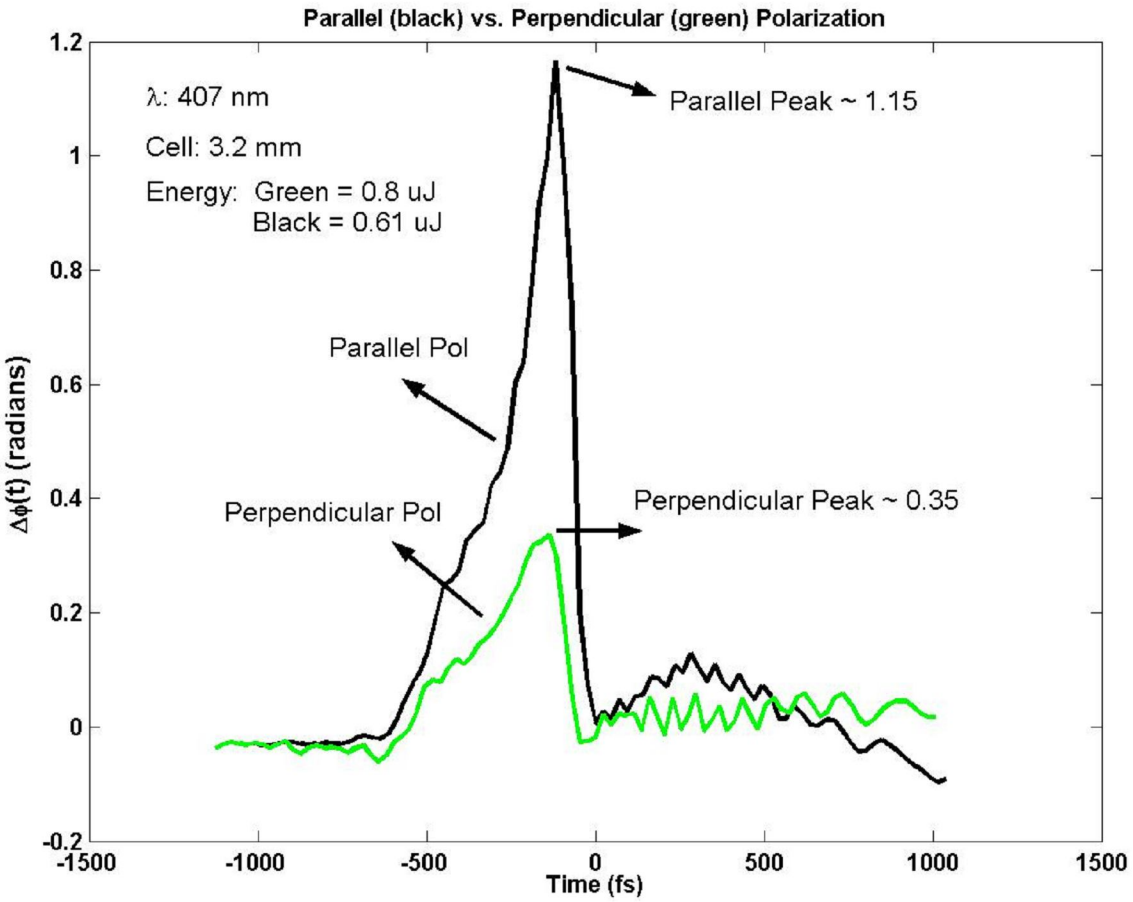

Figure 5.13: 300 shot average of both parallel (black) and perpendicular (green) polarization relative to the SC where $\Delta\phi(x=0,t)_{parallel}/\Delta\phi(x=0,t)_{perpendicular}$ = 3.3. Due to suspected time dependence, correlation to a factor of 3 between parallel and perpendicular polarization cannot be asserted. Times are arbitrary between plots. Both parallel (black) and perpendicular (green) exhibit a ~200 fs ridge on the leading edge. Tail noise of both parallel (black) and perpendicular (green) is independent of pulse as it exists for all of transverse dimension.

Appendix A: Computer Code for Simulation

The following MATLAB code was used to simulate the nonlinear focusing accompanied by group velocity dispersion of the pump beam. The code was written so as to simulate, given initial conditions, three separate events – passing through the front fused silica, water, and rear fused silica. The code for simulating the 815 nanometer light pulse is not included as it is virtually identical with some minor value changes.

```
% Zach Wilkes
% This program models the nonlinear focusing
% of 400 nm light through the front fused silica pane.

% This program is for the front glass of the cell at 400nm
clear
clc

global beta2;
global E;
global k;
global Pnl;

%  Glass thickness of 240 um
z = 0:0.0000024:0.024;

%  **********************  CONSTANTS  ******************

c = 2.997992*10^10;  % speed of light cm/s
n2 = 3.25*10^-16;    % (cm^2/W) Rodriguez, paper Optics Letters v21, #22
n = 1.4696;          % linear index of fused silica 800nm
lambda = 4*10^-5;              % units of cm
k = 2*pi*n/lambda;             % wavenumber
Pnl = 4*lambda^2/(8*pi*n2*n);    % nonlinear Power


%  **********************  INPUTS  **********************

Po = 200*Pnl;        % initial peak power Watts

% initial spot size  0.00269 corresponds to a FWHM of 31.6 um
ro = 0.01274;

% Corresponds to a FWHM pulse length of 90 fs
to = 153*10^-15;

% Initial pulse energy parameter.  NOTE: this  value is
% NOT the actual energy of the pulse
E = Po*to;
```

```
% actual energy in Joules
Energy = E*sqrt(pi/8);

% Full frequency chirp
dlam = 5*10^-7;          % +/- 5nm  in units of cm
dw = 2*pi*c*(1/(lambda+dlam)-1/(lambda-dlam));

% chirp parameter  Given by dw = 4*beta0/to where dw is the full
% frequency chirp.  Unit:  none, negative sign for normal chirp
beta0 =  -(to/4)*dw;

% GVD parameter (s^2/cm) this number is from Sellmeier equation
% and using GVD equation at:
% http : // www.rp - photonics.com/group_velocity_dispersion.html
beta2 = 9.6*10^-28;

% initial beam convergence/divergence slope
dro = 0;

% propogation distance - cell glass is 240 um thick
zf = 0.024;

% Initial rate of change of pulse length given by eqtn 50
% Sprangle et al.
dto = 2*beta2*beta0/to;

%  ***********  Code to pass information DiffEq Solver  **********

% Initial conditions for differential equation solver
icon = [ro dro to dto];

[z,s] = ode23('odetest',z,icon);

radius = s(:,1);
dradius = s(:,2);
time = s(:,3);
dtime = s(:,4);

% ****************************************************************

figure(1)
plot(z,radius/ro,'r',z,time/to,'b');
title('Plot of normalized Radius and Pulse Length through front glass');

rfinal = radius(10001,1)
tfinal = time(10001,1)
drfinal = dradius(10001,1)
Energy

FGradius = radius;
FGpulselen = time;

% This calculates the Irradiance (intensity) of the beam and plots it
Irr = (2*E)./(pi.*(radius).^2.*time);
figure(2)
```

```
plot(z,Irr,'g');
title('Plot of Irradiance (W/cm2) front glass');

PhaseShift = (2/lambda)*n2*(sum(Irr)*0.0000024)

A = [rfinal tfinal drfinal Energy];

%write the final values to a file
fid = fopen('beamparams1.txt', 'wt');  %open the file
fprintf(fid, '%s\n', 'Beam Parameters');   %write the header
fprintf(fid, '%6.14e\n', A);   %write data to file
fclose(fid);   %close file
disp('Write to beamparams1 is successful!... press spacebar to continue')

pause

stuff1(1,:) = FGradius';
stuff1(2,:) = FGpulselen';
stuff1(3,:) = Irr';

%write the final values to a file
fid = fopen('FGbeam.txt', 'wt');  %open the file
fprintf(fid, '%s\n', 'Beam Evolution');   %write the header
fprintf(fid, '%6.6e %6.6e %6.6e\n', stuff1);   %write data to file
fclose(fid);   %close file
disp('Write to FGbeam is successful!... press spacebar to continue')

pause
```

```
% Zach Wilkes
% This program models the nonlinear focusing
% 400 nm light through the water cell

% This program is for the water of the cell at 400nm
clear
clc

global beta2;
global E;
global k;
global Pnl;

% Water thickness of 3.2 mm
z = 0:0.000032:0.32;

% Water Thickness of 1.8 mm
% z = z = 0:0.000018:0.18;

%read the file back in
fid = fopen('beamparams1.txt', 'rt');   %open the file
title1 = fgetl(fid);  %read in the header
B = fscanf(fid, '%22e');   %read in data
fclose(fid);   %close the file

%  **********************  CONSTANTS  ******************

c = 2.997992*10^10;              % speed of light cm/s
n2 = 4.0*10^-16;        % (cm^2/W) n2 for water from paper
n = 1.339;              % linear index of fused silica 800nm
lambda = 4*10^-5;              % units of cm
k = 2*pi*n/lambda;              % wavenumber
Pnl = 4*lambda^2/(8*pi*n2*n);    % nonlinear Power


%  **********************  INPUTS  **********************

Po = 56*Pnl;        % initial peak power Watts

% initial spot size  0.00269 corresponds to a FWHM of 31.6 um
ro = B(1);

% Corresponds to a FWHM pulse length of 90 fs
to = B(2);

% Initial pulse energy parameter.  NOTE: this  value is
% NOT the actual energy of the pulse
E = Po*to;

% actual energy in Joules
Energy = E*sqrt(pi/8);

% Full frequency chirp
dlam = 5*10^-7;          % +/- 5nm  in units of cm
dw = 2*pi*c*(1/(lambda+dlam)-1/(lambda-dlam));
```

```
% chirp parameter  Given by dw = 4*beta0/to where dw is the full
% frequency chirp.  Unit:  none
beta0 =  -(to/4)*dw;

% GVD parameter (s^2/cm) this number is from a measurement
% made by Dr. Ted Jones at NRL.
beta2 = 1.00*10^-27;

% initial beam convergence/divergence slope
dro = B(3);

% propogation distance - cell glass is 240 um thick
zf = 0.32;

% Initial rate of change of pulse length given by eqtn 50
% Sprangle et al.
dto = 2*beta2*beta0/to;

%  ***********  Code to pass information DiffEq Solver  **********

% Initial conditions for differential equation solver
icon = [ro dro to dto];

[z,s] = ode23('odetest',z,icon);

radius = s(:,1);
dradius = s(:,2);
time = s(:,3);
dtime = s(:,4);

% ************************************************************

figure(3)
plot(z,radius/ro,'r',z,time/to,'b');
title('Plot of normalized Radius and Pulse Length through water');

rfinal = radius(10001,1)
tfinal = time(10001,1)
drfinal = dradius(10001,1)
Energy

Wradius = radius;
Wpulselen = time;

% This calculates the Irradiance (intensity) of the beam and plots it
Irr = (2*E)./(pi.*(radius).^2.*time);

figure(4)
plot(z,Irr,'g');
title('Plot of Irradiance (W/cm2) through water');

PhaseShift = (2/lambda)*n2*(sum(Irr)*0.000032)


C = [rfinal tfinal drfinal Energy];
```

```
%write the final values to a file
fid = fopen('beamparams2.txt', 'wt');  %open the file
fprintf(fid, '%s\n', 'Beam Parameters');   %write the header
fprintf(fid, '%6.14e\n', C);   %write data to file
fclose(fid);   %close file
disp('Write of file is successful!... press spacebar to continue')

pause

stuff2(1,:) = Wradius';
stuff2(2,:) = Wpulselen';
stuff2(3,:) = Irr';

%write the final values to a file
fid = fopen('Wbeam.txt', 'wt');  %open the file
fprintf(fid, '%s\n', 'Beam Evolution');   %write the header
fprintf(fid, '%6.6e %6.6e %6.6e\n', stuff2);   %write data to file
fclose(fid);   %close file
disp('Write to Wbeam is successful!... press spacebar to continue')

pause
```

```
% Zach Wilkes
% This program models the nonlinear focusing
% of 800 and 400 nm light in small water cells.

% This program is for the back glass of the cell at 400nm
clear
clc

global beta2;
global E;
global k;
global Pnl;

%  Glass thickness of 240 um
z = 0:0.0000024:0.024;

%read the file back in
fid = fopen('beamparams2.txt', 'rt');   %open the file
title2 = fgetl(fid);  %read in the header
D = fscanf(fid, '%22e');   %read in data
fclose(fid);   %close the file


%  **********************  CONSTANTS  ******************

c = 2.997992*10^10;  % speed of light cm/s
n2 = 3.25*10^-16;    % (cm^2/W) Rodriguez, paper Optics Letters v21, #22
n = 1.4696;          % linear index of fused silica 800nm
lambda = 4*10^-5;              % units of cm
k = 2*pi*n/lambda;             % wavenumber
Pnl = 4*lambda^2/(8*pi*n2*n);    % nonlinear Power


%  **********************  INPUTS  **********************

Po = 195*Pnl;        % initial peak power Watts

% initial spot size  0.00269 corresponds to a FWHM of 31.6 um
ro = D(1);

% Corresponds to a FWHM pulse length of 90 fs
to = D(2);

% Initial pulse energy parameter.  NOTE: this  value is
% NOT the actual energy of the pulse
E = Po*to;

% actual energy in Joules
Energy = E*sqrt(pi/8);

% Full frequency chirp
dlam = 5*10^-7;          % +/- 5nm  in units of cm
dw = 2*pi*c*(1/(lambda+dlam)-1/(lambda-dlam));

% chirp parameter  Given by dw = 4*beta0/to where dw is the full
% frequency chirp.  Unit:  none
```

```
beta0 =  -(to/4)*dw;

% GVD parameter (s^2/cm) this number is from Sellmeier equation
% and using GVD equation at:
% http : // www.rp - photonics.com/group_velocity_dispersion.html
beta2 = 9.6*10^-28;

% initial beam convergence/divergence slope
dro = D(3);

% propogation distance - cell glass is 240 um thick
zf = 0.024;

% Initial rate of change of pulse length given by eqtn 50
% Sprangle et al.
dto = 2*beta2*beta0/to;

%  ***********  Code to pass information DiffEq Solver  **********

% Initial conditions for differential equation solver
icon = [ro dro to dto];

[z,s] = ode23('odetest',z,icon);

radius = s(:,1);
dradius = s(:,2);
time = s(:,3);
dtime = s(:,4);

% ************************************************************

figure(5)
plot(z,radius/ro,'r',z,time/to,'b');
title('Plot of Normalized Radius and Pulse Length through back glass');

rfinal = radius(10001,1)
tfinal = time(10001,1)
drfinal = dradius(10001,1)
Energy

BGradius = radius;
BGpulselen = time;

% This calculates the Irradiance (intensity) of the beam and plots it
Irr = (2*E)./(pi.*(radius).^2.*time);
figure(6)
plot(z,Irr,'g');
title('Plot of Irradiance (W/cm2) through back glass');

PhaseShift = (2/lambda)*n2*(sum(Irr)*0.0000024)

stuff3(1,:) = BGradius';
stuff3(2,:) = BGpulselen';
stuff3(3,:) = Irr';

%write the final values to a file
```

```
fid = fopen('BGbeam.txt', 'wt');  %open the file
fprintf(fid, '%s\n', 'Beam Evolution');    %write the header
fprintf(fid, '%6.6e %6.6e %6.6e\n', stuff3);   %write data to file
fclose(fid);   %close file
disp('Write to BGbeam is successful!... press spacebar to continue')

pause
```

```
%  This program reads in the beam radius and pulse length
%  values as they change through the water cell and plots them


%read Front Glass file back in
fid = fopen('FGbeam.txt', 'rt');   %open the file
title3 = fgetl(fid);  %read in the header
beamplot1 = fscanf(fid, '%14e %14e %14e', [3 inf]);   %read in data
fclose(fid);   %close the file

%read Water file back in
fid = fopen('Wbeam.txt', 'rt');   %open the file
title4 = fgetl(fid);  %read in the header
beamplot2 = fscanf(fid, '%14e %14e %14e', [3 inf]);   %read in data
fclose(fid);   %close the file

%read Back Glass file back in
fid = fopen('BGbeam.txt', 'rt');   %open the file
title5 = fgetl(fid);  %read in the header
beamplot3 = fscanf(fid, '%14e %14e %14e', [3 inf]);   %read in data
fclose(fid);   %close the file

% ****  Plots Radius evolution over the water cell  *****

beamradius1 = beamplot1(1,:);
beamradius2 = beamplot2(1,:);
beamradius3 = beamplot3(1,:);
beamradius = [beamradius1 beamradius2 beamradius3];

z1 = 0:0.0000024:0.024;
z2 = 0.024:2.96*10^-5:0.32;
z3 = 0.32:0.0000024:0.344;

zrr = [z1 z2 z3];

figure(7)
plot(zrr,beamradius,'r');
title('Plot of Radius through entire cell');


%  *****   Plots Pulse Length Evolution over water cell  ****

beamtime1 = beamplot1(2,:);
beamtime2 = beamplot2(2,:);
beamtime3 = beamplot3(2,:);
beamtime = [beamtime1 beamtime2 beamtime3];

figure(8)
plot(zrr,beamtime,'b');
title('Plot of Pulse Length through entire cell');
```

```
% This is the code that computes the radius and pulse length
% from the couple differential equations

function rdot = odetest(z,r)

global beta2;
global E;
global k;
global Pnl;


rdot(4) = (4*beta2*E)/(k*Pnl*r(1)^2*r(3)^2)+4*beta2^2/(r(3)^3);
rdot(3) = r(4);
rdot(2) = 4/(k^2*(r(1))^3)*(1-E/(Pnl*r(3)));
rdot(1) = r(2);

rdot = [rdot(1); rdot(2); rdot(3); rdot(4)];
```

Appendix B: Computer Code for Peak Intensity and n_2 Calculation

```
% This program reads in and averages the .png files
% For the phase extraction code.
% Zach Wilkes   8/1/07

%  NOTE
%  Red Pulse width = 90 fs (FWHM) =>  to = 76.5 1/e^2
%  MAKE SURE TO CHANGE THE ENERGY  !!!!!

N = 7;
sum1 = zeros(480,640);
sum2 = zeros(480,640);

% this loop averages the 7 spot images and creates a new image
% called At7120Spot
for i = 1:N
   name = cat(2,'RedSpot440-',num2str(i));
   filename = cat(2,name,'.png');
   a = double(imread(filename));
   sum1 = sum1+a;
end

RedAt440Spot = sum1./N;

figure(1)
imagesc(RedAt440Spot);

% This code asks the user to select the spot out of the image
% and then creates a new spot

disp('Select Spot in following order Top-Left, Bottom-Right');

bndrs1 = ginput(2);
bndrs1 = round(bndrs1);
newspot = RedAt440Spot(bndrs1(1,2):bndrs1(2,2),bndrs1(1,1):bndrs1(2,1));
newspotsum = sum(sum(newspot))
newspotsize = size(newspot)
newspotx = newspotsize(1);
newspoty = newspotsize(2);
newspotavg = newspotsum/(newspotx*newspoty)

% This code asks the user to select the background which will
% be averaged and subtracted from the spot to get the actual
% light intensity.

disp('Select Small region for background');
bgbndry = ginput(2);
bgbndry = round(bgbndry);

bgspot = RedAt440Spot(bgbndry(1,2):bgbndry(2,2),bgbndry(1,1):bgbndry(2,1));
bgsum = sum(sum(bgspot));
bgsize = size(bgspot);
bgpixnum = bgsize(1)*bgsize(2);
bgavg = bgsum/bgpixnum;
```

```
% This is the sum of the spot minus the background sum
bigsum = newspotsum-(bgavg*newspotx*newspoty)

figure(2)
imagesc(newspot);

%  MAKE SURE TO CHANGE THE ENERGY AND PULSE LENGTH !!!!!!
%  !!!!!!!!!!!!!!!!!!!!
power = sqrt(2/pi)*0.44*10^-6/(76.5*10^-15);   % Power in Watts
K = power/bigsum;                              % Watts per pixel value

peak = K*max(max(newspot));    % Watts represented by peak pixel value
Io = peak/(.51*10^-6)^2        % Peak intensity in Watts/m^2

% This is the n2 value in m^2/W
% MAKE SURE TO CHANGE THE CELL SIZE

n2 = (0.84*(690*10^-9))/((2*pi)*(1.8*10^-3)*(Io))

%  Factor of 2 accounting for XPM

n2pump = .5*n2
```

Appendix C: Perpendicular-Polarization Cross-Phase Modulation Factor

Beginning with third-order polarization at probe frequency (ω_1) in the x-direction:

$$P_x^{(3)}(\omega_1) = K_1(-\omega_1)\varepsilon_o \chi_{xklm}^{(3)}(-\omega_1;\omega_1,-\omega_1,\omega_1)E_k(\omega_1)E_l^*(\omega_1)E_m(\omega_1) + K_2(-\omega_1)\varepsilon_o \chi_{xklm}^{(3)}(-\omega_1;\omega_1,-\omega_2,\omega_2)E_k(\omega_1)E_l^*(\omega_2)E_m(\omega_2) \quad \text{(C.1)}$$

The first term represents the self-phase modulation effect while the second term represents the cross-phase modulation effect. $K_2 = 3/2$ for cross-phase modulation. Also, imagine two waves, a weak probe at ω_1 and a strong pump at ω_2. These can be written such that they have perpendicular polarization:

$$E(\omega_1) = E_x(\omega_1)\hat{x} \quad \text{(C.2)}$$

$$E(\omega_2) = E_y(\omega_2)\hat{y} \quad \text{(C.3)}$$

If $E(\omega_1) << E(\omega_2)$ then Equation C.1 can be reduced to only the cross-phase modulation effect.

$$P_x^{(3)}(\omega_1) = \frac{3}{2}\varepsilon_o \chi_{xklm}^{(3)}(-\omega_1;\omega_1,-\omega_2,\omega_2)E_k(\omega_1)E_l^*(\omega_2)E_m(\omega_2) \quad \text{(C.4)}$$

Expanding the terms:

$$P_x^{(3)}(\omega_1) = \frac{3}{2}\varepsilon_o \Big(\chi_{xxxx}^{(3)}(-\omega_1;\omega_1,-\omega_2,\omega_2)E_x(\omega_1)E_x^*(\omega_2)E_x(\omega_2) + \chi_{xxyy}^{(3)}(-\omega_1;\omega_1,-\omega_2,\omega_2)E_x(\omega_1)E_y^*(\omega_2)E_y(\omega_2) + \chi_{xyxy}^{(3)}(-\omega_1;\omega_1,-\omega_2,\omega_2)E_y(\omega_1)E_x^*(\omega_2)E_y(\omega_2) + \chi_{xyyx}^{(3)}(-\omega_1;\omega_1,\omega_2,-\omega_2)E_y(\omega_1)E_y^*(\omega_2)E_x(\omega_2)\Big) \quad \text{(C.5)}$$

However, several terms are zero therefore:

$$P_x^{(3)}(\omega_1) = \frac{3}{2}\varepsilon_o\left(\chi_{xxyy}^{(3)}(-\omega_1;\omega_1,-\omega_2,\omega_2)E_x(\omega_1)E_y^*(\omega_2)E_y(\omega_2)\right) \quad \text{(C.6)}$$

Applying Kleinman symmetry (far from resonance, nonconducting medium), Isotropic material:

$$\chi_{xxxx} = \chi_{xxyy} + \chi_{xyxy} + \chi_{xyyx} \quad \text{(C.7)}$$

$$\chi_{xxyy} = \chi_{xyxy} = \chi_{xyyx} \quad \text{(C.8)}$$

$$\chi_{xxxx} = 3\chi_{xxyy} \quad \text{(C.9)}$$

$$P_x^{(3)}(\omega_1) = \frac{3}{2}\varepsilon_o\left(\frac{1}{3}\chi_{xxxx}^{(3)}(-\omega_1;\omega_1,\omega_1,-\omega_1)\right)\left|E_y(\omega_2)\right|^2 E_x(\omega_1) \quad \text{(C.10)}$$

Index of refraction for ω_1

$$n^2(\omega_1) = \chi_{eff} + 1 \quad \text{(C.11)}$$

$$n^2(\omega_1) = \chi^{(1)}(-\omega_1;\omega_1) + 1 + \frac{1}{2}\chi_{xxxx}^{(3)}(-\omega_1;\omega_1,\omega_1,-\omega_1)\left|E_y(\omega_2)\right|^2 \quad \text{(C.12)}$$

$$n^2(\omega_1) = n_o^2\left(1 + \frac{1}{2n_o^2}\chi_{xxxx}^{(3)}(-\omega_1;\omega_1,\omega_1,-\omega_1)\left|E_y(\omega_2)\right|^2\right) \quad \text{(C.13)}$$

$$n(\omega_1) = n_o\left(1 + \frac{1}{4n_o^2}\chi_{xxxx}^{(3)}(-\omega_1;\omega_1,\omega_1,-\omega_1)\left|E_y(\omega_2)\right|^2\right) \quad \text{(C.14)}$$

$$n(\omega_1) = n_o + \frac{1}{4n_o}\chi_{xxxx}^{(3)}(-\omega_1;\omega_1,\omega_1,-\omega_1)\left|E_y(\omega_2)\right|^2 \quad \text{(C.15)}$$

$$n(\omega_1) = n_o + \frac{1}{4n_o}\chi_{xxxx}^{(3)}(-\omega_1;\omega_1,\omega_1,-\omega_1)\frac{2I}{n_o\varepsilon_o c} \quad \text{(C.16)}$$

$$n(\omega_1) = n_o + \frac{2}{3}\left(\frac{3}{4}\frac{\chi_{xxxx}^{(3)}(-\omega_1;\omega_1,\omega_1,-\omega_1)}{n_o^2\varepsilon_o c}\right)I \quad \text{(C.17)}$$

$$n(\omega_1) = n_o + \frac{2}{3}n_2 I \quad \text{(C.18)}$$

In Equation C.18, n_2 is the self-phase modulation nonlinear index of refraction. Therefore when a measurement is made by a weak beam at ω_1, the cross-phase modulation by a strong pump ω_2 perpendicular to the weak beam has a factor of 2/3.

Appendix D: Derivation of Linear and Nonlinear Indices of Refraction Using the Classical Anharmonic Oscillator Method

Beginning with the following fundamental equations:

$$P(t) = -(Ne)x(t) \tag{D.1}$$

$$P(t) = \varepsilon_o \chi_e E(t) \tag{D.2}$$

$$F = ma = m\ddot{x}(t) \tag{D.3}$$

$$n_o = \sqrt{1 + \chi^{(1)}} \tag{D.4}$$

where P(t) is the polarization or dipole moment per unit volume, N is the density of atoms per unit volume, x(t) is the time dependent position of the electron, n_o is the linear index of refraction, $\chi^{(1)}$ the linear susceptibility, and χ_e is the effective susceptibility. An anharmonic oscillator under the influence of an external electric field from an optical wave can be modeled the following way:

$$\ddot{x}(t) + 2\gamma\dot{x}(t) + \Omega^2 x(t) = -\frac{e}{m}E(t) \tag{D.5}$$

If E(t) is assumed to be $E_o\cos(t)$ then it can be written as:

$$E(t) = \frac{1}{2}E_o e^{-i\omega t} + \frac{1}{2}E_o e^{+i\omega t} \tag{D.6}$$

inserting into Equation D.5 and solving, then x(t) becomes:

$$x(t) = \frac{-eE_o}{2m}\frac{1}{\Omega^2 - 2i\gamma\omega - \omega^2}e^{-i\omega t} + \frac{-eE_o}{2m}\frac{1}{\Omega^2 + 2i\gamma\omega - \omega^2}e^{+i\omega t} \tag{D.7}$$

Using this to find the linear polarization, $P^{(1)}(t)$ becomes:

$$P^{(1)}(t) = \frac{Ne^2E_o}{2m}\frac{1}{D(\omega)}e^{-i\omega t} + \text{complex conjugate} \tag{D.8}$$

where $D(\omega) = \Omega^2 - 2i\gamma\omega - \omega^2$. Equating Equation D.8 to Equation D.2 then the linear susceptibility at the particular frequency, ω, becomes:

$$\chi^{(1)}(-\omega;\omega) = \frac{Ne^2}{m\varepsilon_o}\frac{1}{D(\omega)} \tag{D.9}$$

Using Equation D.4 this gives the linear index of refraction n_o as:

$$n_o = \left(1 + \frac{Ne^2}{m\varepsilon_o D(\omega)}\right)^{\frac{1}{2}} \tag{D.10}$$

In order to calculate the nonlinear index of refraction first consider an anharmonic oscillator with, instead of a linear restoring force, kx(t), a nonlinear contribution to the restoring force, $k_3x^3(t)$:

$$m\ddot{x}(t) = -eE(t) - \left(k_1 x(t) + k_3 x^3(t)\right) - 2m\gamma\dot{x}(t) \tag{D.11}$$

then using perturbation theory

$$x(t) = x^{(1)}(t) + x^{(3)}(t) \text{ where } x^{(3)}(t) << x^{(1)}(t) \tag{D.12}$$

plugging into Equation D.11

$$\begin{aligned}&\left(\ddot{x}^{(1)}(t) + \ddot{x}^{(3)}(t)\right) + 2\gamma\left(\dot{x}^{(1)}(t) + \dot{x}^{(3)}(t)\right) + \Omega^2\left(x^{(1)}(t) + x^{(3)}(t)\right) + \frac{e}{m}E(\omega) = \\ &-\frac{k_3}{m}\left(x^{(1)}(t) + x^{(3)}(t)\right)^3\end{aligned} \tag{D.13}$$

where E(ω) denotes the complex phasor amplitude associated with the ω frequency, it is not E as a function of ω. Likewise, P(ω) denotes the complex phasor amplitude associated with the polarization. Using complex phasor notation, the electric field and polarization look like:

$$E(t) = \frac{1}{2}E(\omega)e^{-i\omega t} + \frac{1}{2}E^*(\omega)e^{+i\omega t} \tag{D.14}$$

$$P(t) = P^{(1)}(t) + P^{(3)}(t) + \ldots \tag{D.15}$$

$$P^{(1)}(t) = \frac{1}{2}P(\omega)e^{-i\omega t} + \frac{1}{2}P^{*}(\omega)e^{+i\omega t} \tag{D.16}$$

Likening Equation D.16 to D.8, this gives an expression for the linear polarization in terms of the complex phasor amplitude of the electric field and D(ω):

$$P(\omega) = \frac{Ne^2 E(\omega)}{mD(\omega)} \tag{D.17}$$

Going back to Equation D.13 and expanding the terms, it can be seen that the $x^{(1)}(t)$ becomes the driving term for the third-order nonlinearity.

$$\left(\ddot{x}^{(1)}(t) + 2\gamma\dot{x}^{(1)}(t) + \Omega^2 x^{(1)}(t) + \frac{e}{m}E(\omega)\right) + \left(\ddot{x}^{(3)}(t) + 2\gamma\dot{x}^{(3)}(t) + \Omega^2 x^{(3)}(t)\right) = \left(\frac{-k_3}{m}\right)\left(x^{(1)}(t)\right)^3 \tag{D.18}$$

however, the first expression on the left hand side is equal to zero from Equation D.5, resulting in:

$$\left(\ddot{x}^{(3)}(t) + 2\gamma\dot{x}^{(3)}(t) + \Omega^2 x^{(3)}(t)\right) = \left(\frac{-k_3}{m}\right)\left(x^{(1)}(t)\right)^3 \tag{D.19}$$

using the equation for the $x^{(1)}(t)$ from Equation D.6 and expanding it on the right hand side Equation D.19 becomes:

$$\left(\ddot{x}^{(3)}(t) + 2\gamma\dot{x}^{(3)}(t) + \Omega^2 x^{(3)}(t)\right) = \left(\frac{-k_3}{m}\right)\left(\frac{-e}{2m}\right)^3\left(\left(\frac{E(\omega)}{D(\omega)}\right)^3 e^{-3i\omega t} + \left(\frac{E^{*}(\omega)}{D^{*}(\omega)}\right)^3 e^{+3i\omega t} + 3\left(\frac{E^2(\omega)E^{*}(\omega)}{D^2(\omega)D(\omega)}\right)e^{-i\omega t} + 3\left(\frac{E(\omega)\left(E^{*}(\omega)\right)^2}{D(\omega)\left(D^{*}(\omega)\right)^2}\right)e^{+i\omega t}\right) \tag{D.20}$$

The purpose of this is to solve for $x^{(3)}(t)$, use Equation D.1, and provide an equation for $P^{(3)}(t)$. Solving for $x^{(3)}(t)$ gives:

$$x^{(3)}(t) = \frac{3e^3 k_3 E^2(\omega)E^*(\omega)}{8m^4 D^3(\omega)D(3\omega)} e^{-i\omega t} + \frac{e^3 k_3 E^3(\omega)}{8m^4 D^{*3}(\omega)D(3\omega)} e^{-3i\omega t} + CC \qquad \text{(D.21)}$$

$$P^{(3)}(t) = \frac{1}{2} Ne\left(\frac{-3e^3 k_3 E^2(\omega)E^*(\omega)}{4m^4 D^3(\omega)D^*(\omega)} \right) e^{-i\omega t} + \frac{1}{2} Ne\left(\frac{-e^3 k_3 E^3(\omega)}{4m^4 D^3(\omega)D(3\omega)} \right) e^{-3i\omega t} + CC \qquad \text{(D.22)}$$

$$P^{(3)}(t) = \frac{1}{2} P^{(3)}(\omega) e^{-i\omega t} + \frac{1}{2} P^{(3)}(3\omega) e^{-3i\omega t} + CC \qquad \text{(D.23)}$$

where CC = complex conjugate. From this it can be seen that $P^{(3)}(t)$ contains an ω and 3ω component. The optical Kerr effect, the ω component, is responsible for self-focusing, self-phase modulation, and other effects. The total polarization at frequency ω can written as the sum of the linear polarization at frequency ω and the nonlinear third-order polarization at frequency ω, in other words:

$$P_{total}(\omega) = P^{(1)}(\omega) + P^{(3)}(\omega) \qquad \text{(D.24)}$$

It is possible to define by inspection (a more rigorous proof will not be done here, please see Boyd[7]) by using Equations D.23 and D.2 the third-order nonlinear polarization at frequency ω as:

$$P^{(3)}(\omega) = \frac{3\varepsilon_o}{4} \chi^{(3)}(-\omega;\omega,-\omega,\omega) E(\omega)E^*(\omega)E(\omega) \qquad \text{(D.25)}$$

solving for $\chi^{(3)}(-\omega;\omega,-\omega,\omega)$:

$$Ne \frac{-3e^3 k_3 E^2(\omega)E^*(\omega)}{4m^4 D^3(\omega)D^*(\omega)} = \frac{3\varepsilon_o}{4} \chi^{(3)}(-\omega;\omega,-\omega,\omega) E(\omega)E^*(\omega)E(\omega) \qquad \text{(D.26)}$$

$$\chi^{(3)}(-\omega;\omega,-\omega,\omega) = \frac{-Ne^4 k_3}{m^4 \varepsilon_o D^3(\omega)D^*(\omega)} \qquad \text{(D.27)}$$

Using Equation D.24 and the proposed definitions of the linear and nonlinear susceptibilities at frequency ω, the total polarization at frequency ω, for linearly polarized

E(ω) and P(ω) can be written as:

$$P_{total}(\omega) = \varepsilon_o \chi^{(1)}(-\omega;\omega)E(\omega) + \frac{3}{4}\varepsilon_o \chi^{(1)}(-\omega;\omega,-\omega,\omega)E(\omega)E^*(\omega)E(\omega) \quad \text{(D.28)}$$

$$P_{total}(\omega) = \left(\varepsilon_o \chi^{(1)}(-\omega;\omega) + \frac{3}{4}\varepsilon_o \chi^{(1)}(-\omega;\omega,-\omega,\omega)E(\omega)E^*(\omega) \right) E(\omega) \quad \text{(D.29)}$$

$$P_{total}(\omega) = \varepsilon_o \chi_{total} E(\omega) \quad \text{(D.30)}$$

$$n = \left(1 + \chi_{total}\right)^{\frac{1}{2}} \quad \text{(D.31)}$$

$$n = \left(1 + \chi^{(1)} + \frac{3}{4}\chi^{(3)} E(\omega)E^*(\omega) \right)^{\frac{1}{2}} \quad \text{(D.32)}$$

$$n \approx \left(1 + \chi^{(1)}\right)^{\frac{1}{2}} + \frac{1}{2}\left(1 + \chi^{(1)}\right)^{\frac{-1}{2}} \left(\frac{3}{4}\chi^{(3)} \right) E(\omega)E^*(\omega) \quad \text{(D.33)}$$

$$n = n_o + \left(\frac{3}{4}\chi^{(3)} \right)\left(\frac{1}{n_o} \right)\left(\frac{1}{2}E(\omega)E^*(\omega) \right) \quad \text{(D.34)}$$

$$n = n_o + \left(\frac{3}{4}\chi^{(3)} \right)\left(\frac{n_o}{n_o^2} \right)\left(\frac{\varepsilon_o c}{\varepsilon_o c} \right)\left(\frac{1}{2}E(\omega)E^*(\omega) \right) \quad \text{(D.35)}$$

$$n = n_o + \left(\frac{3}{4} \right)\left(\frac{\chi^{(3)}}{n_o^2 \varepsilon_o c} \right)\left(\frac{1}{2} n_o \varepsilon_o c \left|E(\omega)\right|^2 \right) \quad \text{(D.36)}$$

$$n = n_o + n_2 I \quad \text{(D.37)}$$

where n_2 represents the nonlinear index of refraction in units of cm^2/W and I is the intensity of the optical.

$$n_2 = \frac{3\chi^{(3)}(-\omega;\omega,-\omega,\omega)}{4 n_o^2 \varepsilon_o c} \quad \text{(D.38)}$$

$$I = \frac{1}{2} n_o \varepsilon_o c \left|E(\omega)\right|^2 \quad \text{(D.39)}$$

Appendix E: Calculations Pertinent to Temperature Effect

The power absorbed by the water cell is:

$$P_{abs} = P_{in}\left(1 - e^{-\alpha z}\right) \tag{E.1}$$

for a window of 3.2 mm then

$$P_{abs} = \left(5.56x10^{7}\right)\left(1 - e^{-(2.07)*(0.0032)}\right) = 367000\frac{J}{s} \tag{E.2}$$

$$\left(3.67x10^{5}\, J/s\right)*(90\, fs) = 3.3x10^{-8}\, Joules \tag{E.3}$$

The specific heat capacity of water is C = 4.184 J/g/^{o}C

Using the heat change formula will give the change in temperature of some mass of water for a given amount of energy:

$$\Delta Q = mC\Delta T \tag{E.4}$$

The mass of water to be heated:

$$m = \rho V = \left(\frac{1gram}{cm^{3}}\right)\left(3.2mm*\pi*\left(60\mu m\right)^{2}\right) \tag{E.5}$$

m = 36.2 micrograms.

The change in index of refraction, Δn, from change in temperature, ΔT is calculated where δn/^{o}C = 9.85x10^{-5} from [2]:

$$\Delta T = \frac{\Delta Q}{mC} = \frac{3.3x10^{-8}\, J}{36.2\mu g*4.184 J/g/^{o}C} = 0.000218 \tag{E.6}$$

$$\Delta n = \left(\frac{\delta n}{^{o}C}\right)\left(0.000218^{o}C\right) = \left(9.85x10^{-5}\right)\left(0.000218^{o}C\right) \tag{E.7}$$

this gives a change in index of refraction of Δn = 2.15x10^{-8}.

Appendix F: Red and Blue Pulse Spectra and SHG Crystal Efficiency

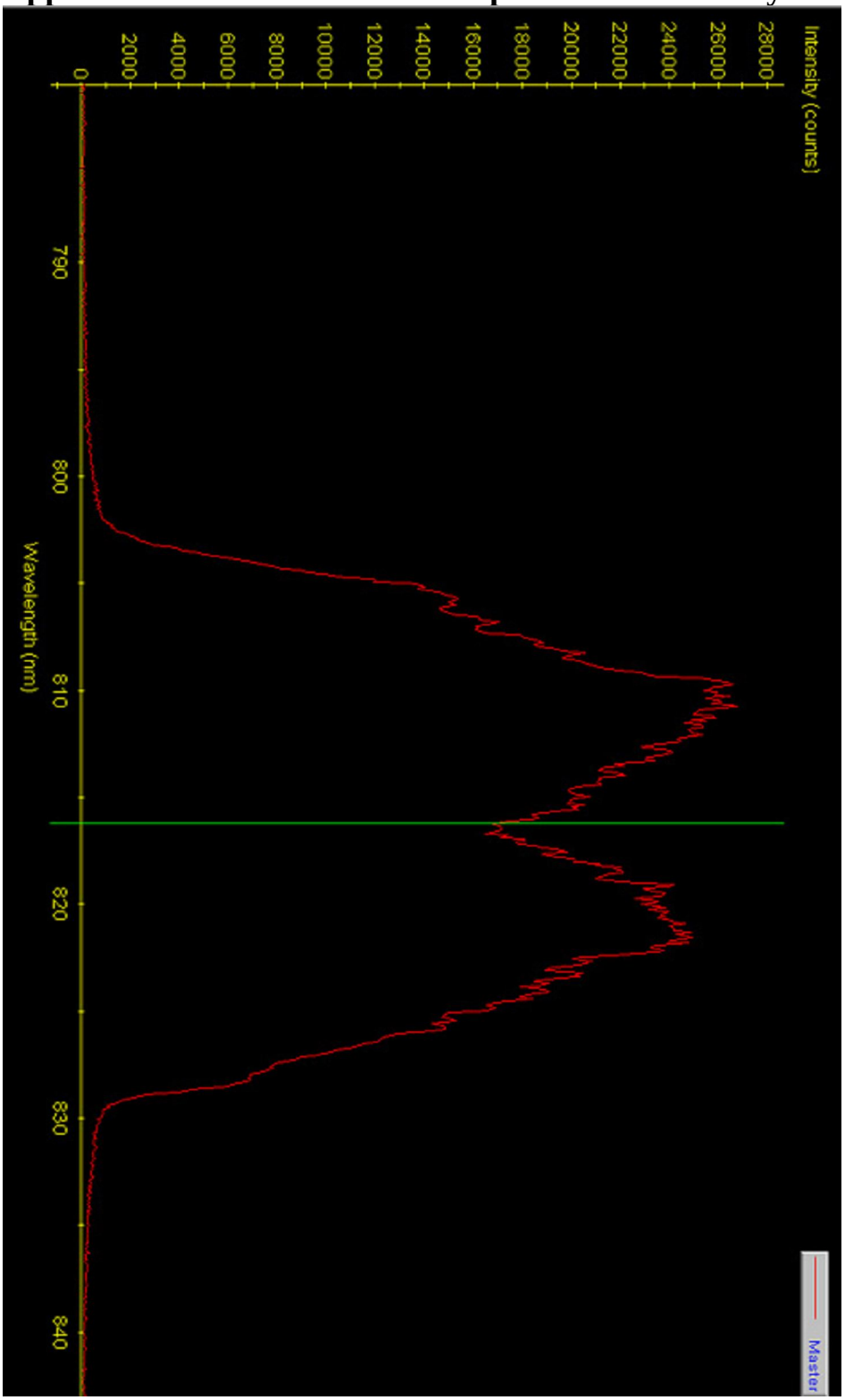

Figure F.1: Spectrum of the red (815 nm) pulse used in the experiment.

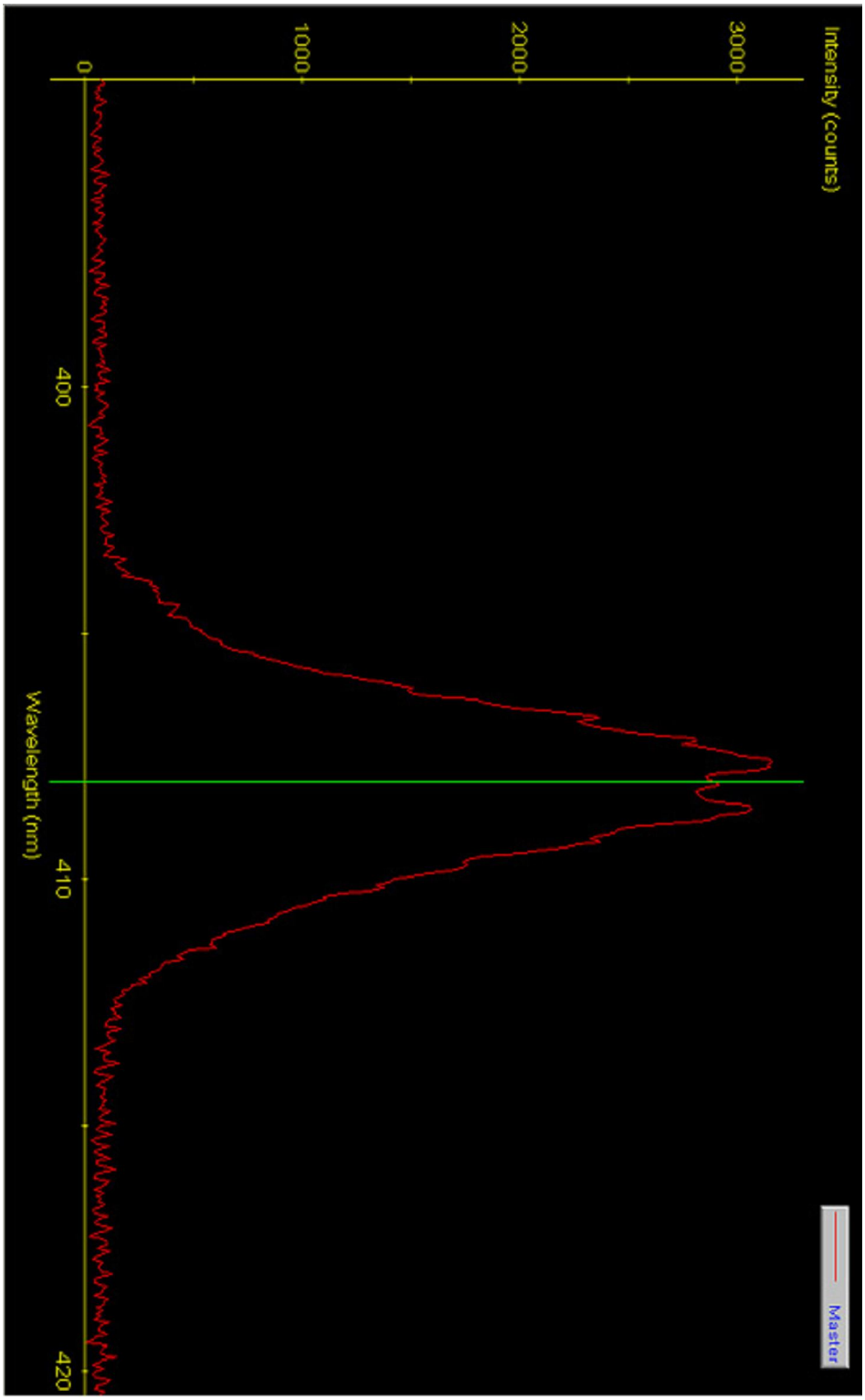

Figure F.2: This is the spectrum of the blue (407 nm) light used in the experiment.

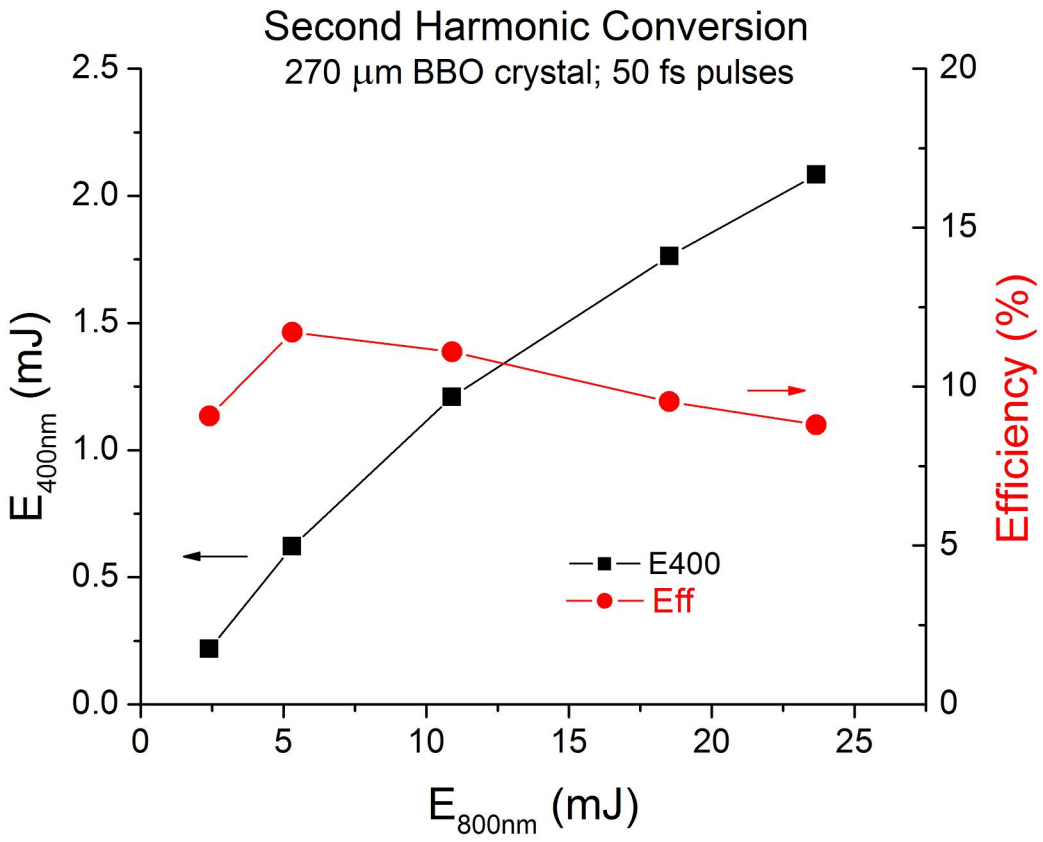

Figure F.3: Second harmonic generation efficiency of the 270 μm BBO crystal used to generate 407 nm light in the experiment.

Appendix G: Water Cell Housing Schematics and 3-D CAD Drawing

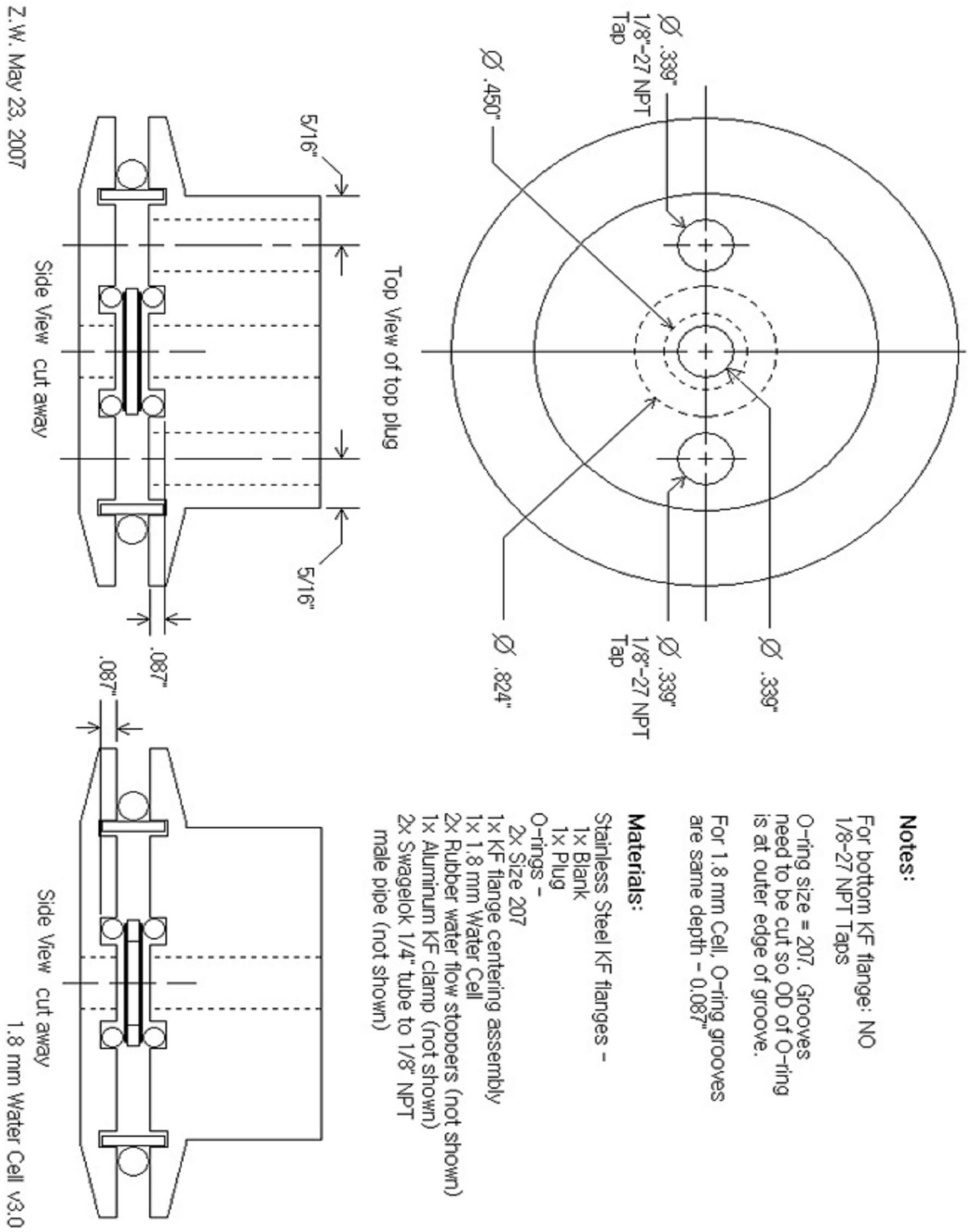

Figure G.1: A schematic of the stainless steel water cell housing cut to hold the 1.8 mm water cell. It is made by compressing 2 stainless steel KF flanges with grooves, .087" deep cut for size 207 O-rings which seal against the water cell windows preventing leaking.

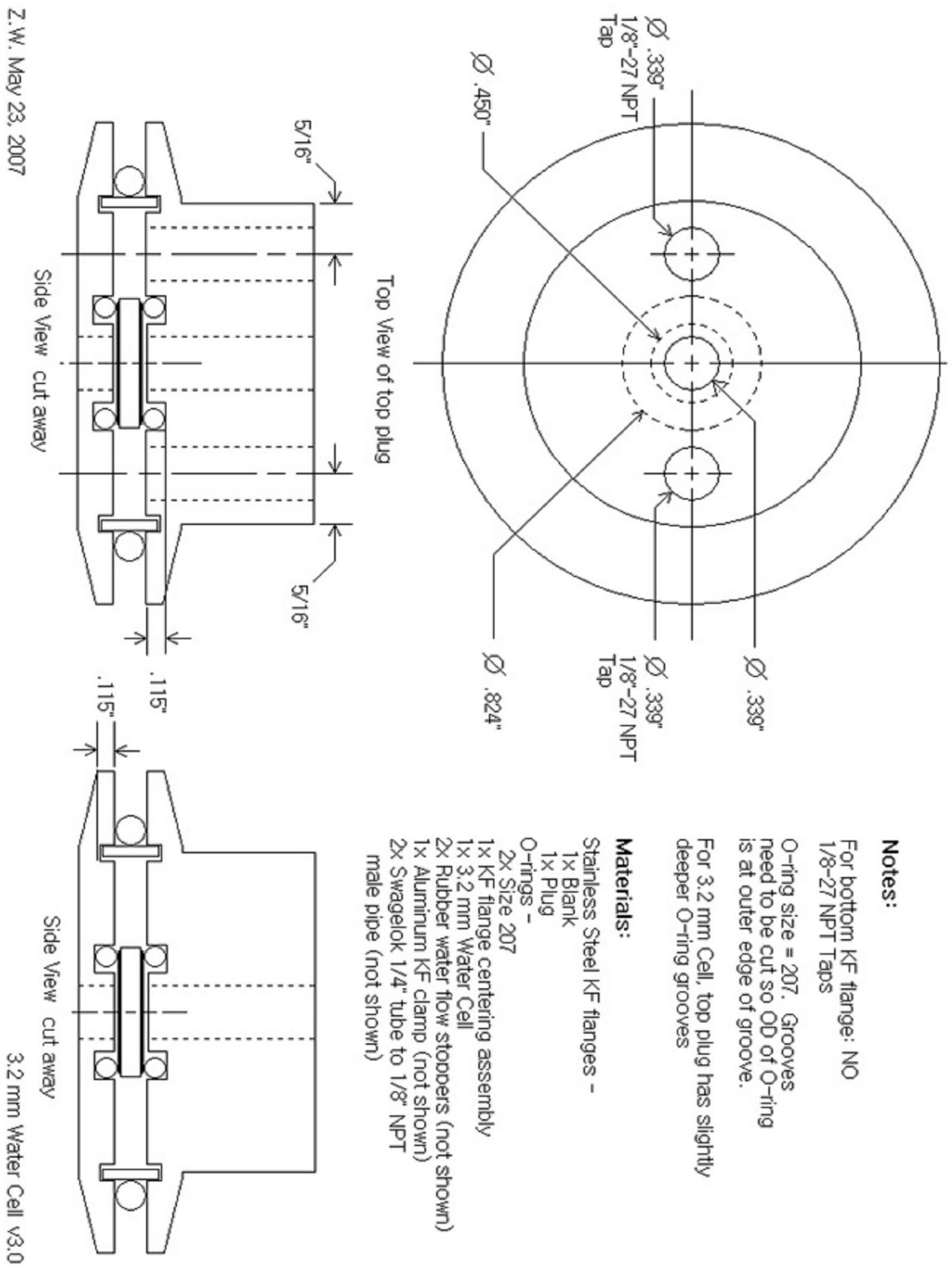

Figure G.2: A schematic of the stainless steel water cell housing cut to hold the 3.2 mm water cell. It is made by compressing 2 stainless steel KF flanges with grooves cut 0.115" deep for size 207 O-rings which seal against the water cell windows preventing leaking.

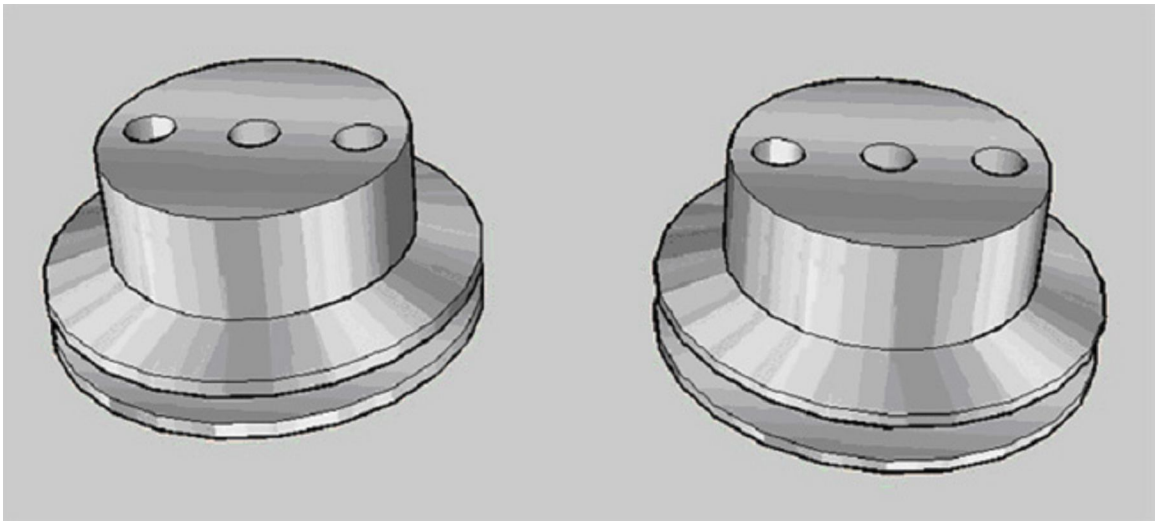

Figure G.3: 3-D rendering of the WCH. The 1.8 mm WC is on the left, 3.2 mm WC on the right.

Appendix H: GVD Calculation for Propagation in Water

From Agarawal[20] the spread in pulse length from dispersion can be calculated using:

$$T_1 = \left(\left(1 + \frac{C\beta_2 z}{T_o^2} \right)^2 + \left(\frac{\beta_2 z}{T_o^2} \right)^2 \right)^{1/2} T_o \qquad \text{(H.1)}$$

where C = chirp parameter, β_2 = group velocity dispersion coefficient, T_1 = 1/e half-width pulse duration due to dispersion, T_o = 1/e half-width initial pulse duration. The experimental FWHM pump pulse lengths are $T_{o\text{-red}}$ = 90 fs, $T_{o\text{-blue}}$ = 250 fs. The GVD coefficients for the red and blue pulses are given in Table 3.1. Conversion from FWHM pulse lengths to 1/e half-width is $T_{FWHM} = 1.665 * T_o$. For both pulses there is no chirping therefore C = 0.

For the red pulse T_o = 54 fs and the percentage change is:

$$\frac{T_1}{T_o} = \left(1 + \left(\frac{\beta_2 z}{T_o^2} \right)^2 \right)^{1/2} = \left(1 + \left(\frac{\left(24.8 \frac{fs^2}{mm} \right)(3.2mm)}{(54\,fs)^2} \right)^2 \right)^{1/2} = 1.00037 \qquad \text{(H.2)}$$

For the blue pulse T_o = 150 fs and the percentage change is:

$$\frac{T_1}{T_o} = \left(1 + \left(\frac{\beta_2 z}{T_o^2} \right)^2 \right)^{1/2} = \left(1 + \left(\frac{\left(100 \frac{fs^2}{mm} \right)(3.2mm)}{(150\,fs)^2} \right)^2 \right)^{1/2} = 1.0001 \qquad \text{(H.3)}$$

List of References

[1] Smith R.C and Baker, K.S., Applied Optics, Vol 20, No. 2, 1981

[2] Schrieber et al. J Phys. Chem. Ref. Data, Vol 19, 1990

[3] Liu et al. Appl. Phys. B 76, 215–229 (2003)

[4] Wikipedia Reynolds Number http://en.wikipedia.org/wiki/Reynolds_number

[5] Wikipedia Tensile strength http://en.wikipedia.org/wiki/Tensile_strength

[6] Sprangle, P., J. R. Peñano, B. Hafizi; "Propagation of Intense Short Laser Lulses in the Atmosphere"; Physcial Review E 66, October 2002

[7] Boyd, Robert W.; *Nonlinear Optics*; Academic Press, 2003

[8] Butcher and Cotter, *The Elements of Nonlinear Optics*; Cambridge University Press, 1990

[9] Noack, J., A. Vogel; "Laser-Induced Plasma Formation in Water at Nanosecond to Femtosecond Time Scales: Calculation of Thresholds, Absorption Coefficients, and Energy Density"; IEEE Journal of Quantum Electronics; Vol. 35, Nl. 8, August 1999

[10] Noack, J., A. Vogel et al.; "Energy balance of optical breakdown in water at nanosecond to femtosecond time scales"; Appl. Phys. B 68, 271–280 (1999)

[11] P. B. Corkum, C. Rolland, and T. Srinivasan-Rao, "Supercontinuum Generation in Gases," Phys. Rev. Lett. 57, 2268-2271 (1986)

[12] Y.-H. Chen, S. Varma, I. Alexeev, and H. M. Milchberg; "Measurement of transient nonlinear refractive index in gases using xenon supercontinuum single-shot spectral interferometry"; Opt. Express; Vol. 15, No. 12; June 2007

[13] K. Y. Kim, I. Alexeev, and H. M. Milchberg; "Single-shot Supercontinuum Spectral Interferometry"; Appl. Phys. Letters; Vol. 81, No. 22, November 2002

[14] Koechner, W; *Solid-State Laser Engineering*; Springer 2006; pp. 202

[15] E. T. J. Nibbering,* G. Grillon, M. A. Franco, B. S. Prade, and A. Mysyrowicz; J. Opt. Soc. Am. B/ Vol. 14, No. 3/March 1997

[16] D.M. Pennington, et al.; "Nonlinear Index of Air at 1.053 um"; Phys. Rev. A, Vol. 39, No. 6; March 1989

[17] Y. Shimoji, A. T. Fay, R. S. F. Chang, and N. Djeu; "Direct measurement of the nonlinear refractive index of air"; J. Opt. Soc. Am. B 6, 1994 (1989).

[18] M. J. Shaw, C. J. Hooker, and D. C. Wilson; ''Measurement of the nonlinear refractive index of air and other gases at 248 nm,'' Opt. Commun. 103, 153 (1993).

[19] A. Brodeur and S. L. Chin; "Band-Gap Dependence of the Ultrafast White-Light Continuum"; P.R. Letters, Vol. 80, No. 20; May 1998

[20] G. Agarawal; *Fiber-Optic Communications Systems*; Wiley and Sons, 2002; pp. 47-48

[21] A. J. Taylor, G. Rodriguez, T. S. Clement; "Determination of n2 by direct measurement of the optical phase"; Opt. Letters, Vol. 21, No. 22; November 15, 1996

[22] Y.-H. Chen, S. Varma, A. York, and H. M. Milchberg; "Single-shot, space- and time-resolved measurement of rotational wavepacket revivals in H_2, D_2, N_2, O_2, and N_2O"; Opt. Express, Vol. 15, No. 18, September 2007.

[23] McMorrow, D. et al; "Femtosecond Optical Kerr Studies on the Origin of the Nonlinear Responses in Simple Liquids"; IEEE Journal of Quantum Electronics, Vol. 24, No. 2, February 1988

[24] Tzer-Hsiang Huang et al.; "The Transient Optical Kerr Effect of Simple Liquids Studied with an Ultrashort Laser with Variable Pulsewidth"; IEEE Journal of Selected Topics in Quantum Electronics, Vol. 2, No. 3, September 1996

[25] Ki-Yong Kim; "Measurement of Ultrafast Dynamics in the Interaction of Intense Laser Pulses with Gases, Atomic Clusters, and Plasmas"; Ph.D Thesis; University of Maryland 2003.

[26] Jackson, J. D.; *Classical Electrodynamics*; 3rd Ed.; Wiley and Sons, 1999

[27] Fowles, Grant R.; *Introduction to Modern Optics*; 2nd Ed; Dover Pub. Inc. 1975

[28] Pope, Robin M. and E. Fry; "Absorption spectrum (380–700) nm of pure water"; Applied Optics; Vol. 36, No. 33; November 1997

[29] http://www.rp-photonics.com/group_velocity_dispersion.html

[30] P. O'Shea et al; "Highly simplified device for ultrashort-pulse measurement"; Optics Letters, Vol. 26, Issue 12, pp. 932-934